

CrystEngComm

Accepted Manuscript



This is an *Accepted Manuscript*, which has been through the Royal Society of Chemistry peer review process and has been accepted for publication.

Accepted Manuscripts are published online shortly after acceptance, before technical editing, formatting and proof reading. Using this free service, authors can make their results available to the community, in citable form, before we publish the edited article. We will replace this *Accepted Manuscript* with the edited and formatted *Advance Article* as soon as it is available.

You can find more information about *Accepted Manuscripts* in the [Information for Authors](#).

Please note that technical editing may introduce minor changes to the text and/or graphics, which may alter content. The journal's standard [Terms & Conditions](#) and the [Ethical guidelines](#) still apply. In no event shall the Royal Society of Chemistry be held responsible for any errors or omissions in this *Accepted Manuscript* or any consequences arising from the use of any information it contains.

³⁵Cl Solid-State NMR of HCl Salts of Active Pharmaceuticals Ingredients: Structural Prediction, Spectral Fingerprinting and Polymorph Recognition

Marcel Hildebrand,[†] Hiyam Hamaed,[†] Andrew M. Namespetra,[†] John M. Donohue,[†] Riqiang Fu,[‡] Ivan Hung,[‡] Zhehong Gan[‡] and Robert W. Schurko^{†,*}

* Author to whom correspondence should be addressed

[†] *Department of Chemistry and Biochemistry, University of Windsor,
Windsor, Ontario, Canada N9B 3P4*

[‡] *National High Magnetic Field Laboratory, 1800 E. Paul Dirac Drive,
Tallahassee, FL 32310 – 3706*

Fax: (519) 973-7098. E-mail: rschurko@uwindsor.ca

Version 1 – requested revisions, April 10, 2014

Abstract

A series of HCl salts of active pharmaceutical ingredients (APIs) have been characterized via ^{35}Cl solid-state NMR (SSNMR) spectroscopy and first-principles plane-wave density functional theory (DFT) calculations of ^{35}Cl NMR interaction tensors. ^{35}Cl NMR spectra have been acquired at both standard (9.4 T) and high (21.1 T) magnetic field strengths, on stationary samples and under conditions of magic-angle spinning (MAS). The ^{35}Cl electric field gradient (EFG) and chemical shift (CS) tensor parameters are readily extracted from analytical simulations of these spectra. These parameters are distinct for each sample, indicating that these spectra can be used as fingerprints for identifying unique solid phases. It is possible to correlate the ^{35}Cl EFG parameters (the quadrupolar coupling constant, C_Q , and the asymmetry parameter, η_Q) to the hydrogen-bonding environments of each chlorine anion, and several simple trends are observed. ^{35}Cl EFG tensors obtained from plane-wave DFT calculations are found to be in good agreement with experiment, and unique structural insights are gained by considering the predicted EFG tensor orientations and the signs of the quadrupolar coupling constants. ^{35}Cl SSNMR can be easily applied for the differentiation of polymorphs of HCl APIs, since the spectra are sensitive to even the subtlest changes in the chlorine anion environments. We discuss the application of this combination of techniques as both standalone and complementary NMR crystallography methodologies for structural characterization and potential high-throughput screening of polymorphs of HCl APIs.

Introduction

Most pharmaceuticals (ca. 80%) are manufactured, shipped, stored, dispensed and ingested as solids,¹ and approximately 80% of known active pharmaceutical ingredients (APIs) exhibit polymorphism² or pseudopolymorphism.³⁻⁷ A chemical substance is said to be polymorphic when it is able to crystallize in more than one form or arrangement, or pseudopolymorphic when it can crystallize in one or more forms as a solvate or hydrate. The identification and differentiation of polymorphs are of great importance in the pharmaceutical industry owing to the unique properties that each pharmaceutical polymorph possesses,⁸⁻¹¹ such as biological activity,¹² solubility,^{13,14} stability^{15,16} and bioavailability.¹⁵⁻¹⁷ In addition, pharmaceutical polymorphs are subject to intellectual property and patenting rights.⁸ Hence, the accurate and rapid analysis of the solid-state structures of APIs is imperative.

The methods most commonly used for the characterization of solid APIs and their polymorphs are single-crystal and powder X-ray diffraction (XRD).^{8,18} In many cases, it can be difficult or even impossible to isolate single crystals of sufficient quality for scXRD experiments. Although pXRD is useful for distinguishing polymorphs, there are limitations to the amount of information that can be procured from powder XRD patterns.^{19,20} In addition, if the solid API is amorphous in nature (i.e., absence of long range molecular/atomic order) it is not feasible to use XRD techniques for detailed structural characterization.

One- and two-dimensional solution-state NMR experiments allow for the structural elucidation of APIs and detection of impurities in the solution phase, but obviously play no role in the structural characterization of their solid forms.²¹⁻²³ Solid-state NMR (SSNMR) spectroscopy is an excellent tool for the characterization of complex APIs and their associated polymorphs, and is often used in a complementary fashion with XRD methods.²⁴⁻³⁰ SSNMR can

provide a great amount of detail on the local chemical structure, detecting differences in bond lengths and angles, local site geometries and other inter- and intramolecular interactions.

SSNMR is also capable of characterizing amorphous compounds, and in turn, is able to differentiate polymorphs with disordered solid-state structures (or even mixtures of crystalline and amorphous substances).²⁵

¹³C SSNMR experiments are the most commonly used for the structural characterization of pharmaceuticals, as well as for the determination of dynamical behavior and the analysis of amorphous phases.^{1, 26, 31-38} Multinuclear SSNMR studies of nuclides such as ¹H, ²H, ¹⁵N, ³¹P, ¹⁹F and ²³Na have also played an important role in the structural elucidation of many common pharmaceuticals, as well as for the detection of polymorphism when ¹³C NMR spectra are ambiguous.³⁹⁻⁴⁶ Two-dimensional homo- and heteronuclear correlation SSNMR experiments have also been applied to the structural characterization of pharmaceuticals for the purpose of determining the chemical bonding and molecular conformations.⁴⁷⁻⁵¹

Since HCl APIs comprise ca. 50% of solid pharmaceuticals,^{52, 53} ³⁵Cl SSNMR is a logical choice for the analysis for their characterization. We previously demonstrated that ³⁵Cl SSNMR spectroscopy is a powerful technique for the study of pharmaceuticals and their polymorphs, as either a complementary tool to pXRD and ¹³C SSNMR spectroscopy, or as an independent source of structural data.⁵⁴ ³⁵Cl SSNMR can provide information on the number of chlorine sites, as well as identifying sites in amorphous/disordered samples or even impurity phases; this is particularly useful in cases where the ¹³C SSNMR spectra or pXRD data are unable to clearly differentiate polymorphs.

Chlorine has two NMR active isotopes, ³⁵Cl and ³⁷Cl. They are both half-integer nuclear spin ($I = 3/2$), quadrupolar nuclei ($Q(^{35}\text{Cl}) = -0.082 \times 10^{-28} \text{ m}^2$ and $Q(^{37}\text{Cl}) = -0.065 \times 10^{-28}$

m^2).^{55, 56} Despite their high natural abundances (75.53% and 24.47% for ^{35}Cl and ^{37}Cl , respectively) they are considered to be unreceptive nuclei due to their low gyromagnetic ratios. SSNMR of ^{35}Cl is preferred, due to its higher receptivity, which largely arises from its higher natural abundance. The ^{35}Cl quadrupolar parameters are highly sensitive to local structural changes, which, in turn, are reflected in their SSNMR spectra. Careful acquisition of ^{35}Cl central-transition (CT, $+1/2 \leftrightarrow -1/2$) powder patterns allows for accurate elucidation of the ^{35}Cl electric field gradient (EFG) parameters: the quadrupolar coupling constant, C_Q , and the asymmetry parameter, η_Q . In addition, it is sometimes possible to obtain the chemical shift (CS) tensor parameters: the isotropic shift, δ_{iso} , the span, Ω , and skew, κ , as well as the Euler angles (α , β , γ) that describe the relative orientations of the CS and EFG tensors,⁵⁷ which can also be correlated to structure (explicit definitions of these parameters are provided in Table 1). Bryce and co-workers have also demonstrated the usefulness of ^{35}Cl SSNMR for studying solid-state structures of other organic systems containing chlorine anions (i.e., HCl salts of amino acids).⁵⁸⁻⁶⁰ In addition, they have demonstrated the ability of ^{35}Cl SSNMR to differentiate pseudopolymorphs of alkaline earth metal chlorides.⁶¹ We refer the reader to the articles by Bryce et al. that discuss the many applications of ^{35}Cl SSNMR.⁶²⁻⁶⁵

Due to recent advances in computational software and associated hardware, density functional theory (DFT) calculations of NMR interaction tensors are of increasing interest, aiding experimental NMR methods in structural elucidation and spectral assignment. Recently, plane-wave DFT methods capable of treating extended structures of periodic solids have been developed and widely deployed, such as the CASTEP⁶⁶⁻⁶⁹ program which utilizes the gauge-including projector augmented wave algorithm (GIPAW).⁶⁶ Theoretical NMR interaction

tensors derived from calculations on periodic solids are of particular value for the study of solid polymorphs.

Herein, we describe the extension of our research to a variety of HCl APIs. Using magic-angle spinning (MAS) NMR, static wide-line NMR and pXRD, in conjunction with plane-wave DFT calculations, we present a comprehensive structural characterization of seventeen different HCl APIs (**Scheme 1**). We establish that ^{35}Cl SSNMR spectroscopy can rapidly and accurately probe chlorine anion environments in APIs, and explore the use of plane-wave DFT calculations as an alternative to more traditional molecular-orbital calculations conducted in previous studies. The majority of this work is focused on systems for which crystal structures are known, in order to identify relationships between the ^{35}Cl EFG tensor parameters and the local Cl^- environments for common structural motifs, via plane-wave DFT calculations. Our new data, in combination with data from our previous work,⁵⁴ and data on HCl salts of amino acids from Wasylshen and Bryce,⁵⁸⁻⁶⁰ is used to validate these relationships, and initiate a database of ^{35}Cl quadrupolar parameters that can be used for structural identification and differentiation. We then demonstrate the application of these methods to two systems with structural polymorphs. Finally, we propose these methodologies as a potential means for investigation of the many classes of APIs, via new NMR crystallography methods, and especially as a fingerprinting tool during drug processing and manufacture, which would be of great value for quality and assurance in the pharmaceutical industry.

Experimental

Samples. Samples of Adip, Bufl, Dicy, Trig, Rani, Dibn, Scop, Mexi, Brom, Alpr, Isop, Aceb, Aman, Proc, Isox, Dopa and Amin were purchased from Sigma Aldrich and used without further purification (full names and molecular formulae are given in **Scheme 1**). Details of the generation of polymorphs MexiI, MexiII and IsoxI are given in the Supporting Information.

Solid-State NMR at 9.4 T. ^{35}Cl and ^{13}C SSNMR experiments were performed on a Varian Infinity Plus NMR spectrometer with an Oxford 9.4 T ($\nu_0(^1\text{H}) = 399.73$ MHz) wide bore magnet with $\nu_0(^{35}\text{Cl}) = 39.26$ MHz and $\nu_0(^{13}\text{C}) = 100.52$ MHz. For ^{35}Cl SSNMR experiments, all samples were packed into 5 mm outer diameter (o.d.) glass tubes and a Varian/Chemagnetics 5 mm HXY MAS probe was used for all experiments. ^{35}Cl chemical shifts were referenced with respect to NaCl (s) ($\delta_{\text{iso}} = 0.00$ ppm).^{60, 64} For ^{13}C SSNMR experiments, all samples were packed into 4 mm o.d. zirconia rotors and a Varian/Chemagnetics 4 mm HX MAS probe was used for all experiments. ^{13}C chemical shifts were referenced to tetramethylsilane ($\delta_{\text{iso}} = 0.00$ ppm), using the high-frequency peak of adamantane as a secondary reference ($\delta_{\text{iso}} = 38.57$ ppm).

^{35}Cl NMR experiments were conducted using a Hahn-echo pulse sequence with a pulse delay of 0.5 s, and a central-transition selective $\pi/2$ pulse width between 1.00 and 7.00 μs (ν_1 between 18 and 125 kHz). A proton-decoupling field of ca. 50 kHz was used in all experiments. In cases where NMR powder patterns are too broad to be uniformly excited with a single, rectangular, high power pulse, spectra were acquired by stepping the transmitter frequency across the entire CT powder pattern in even increments, Fourier transforming the FID from each experiment, and co-adding the individual sub-spectra to produce the final powder pattern.^{70, 71} ^{13}C NMR spectra were acquired using the variable-amplitude cross-polarization (VACP/MAS) technique.⁷² $^1\text{H} \rightarrow ^{13}\text{C}$ VACP/MAS experiments were performed on all samples and the TPPM⁷³

decoupling sequence was employed with a proton decoupling rf power of ca. 63 kHz. These experiments utilized a $\pi/2(^1\text{H})$ pulse width of 2.4 μs (which corresponds to a rf of 104 kHz), a contact time between 1.0 and 5.0 ms, a pulse delay between 1.0 and 2.0 s, a spectral width of 50 kHz, and ν_{rot} of 9.5 and 13 kHz. Full experimental details can be found in the Supporting Information (**Tables S1 – S3, S10**).

Solid-State NMR at 21.1 T. High-field NMR experiments were performed on an ultra-wide bore 900 MHz (21.1 T) superconducting NMR magnet at the NHMFL in Tallahassee, Florida, for which $\nu_0(^{35}\text{Cl}) = 88.13$ MHz. For static ^{35}Cl NMR experiments, samples were packed in rectangular glass containers (7.5 \times 5 \times 11 mm) and spectra were acquired using a low-E rectangular-flat coil HX probe.⁷⁴ MAS experiments, and some of the static NMR experiments, were performed on a on a home-built HX 3.2 mm probe.

^{35}Cl MAS and static NMR experiments were conducted using a Hahn-echo pulse sequence with optimized recycle delays between 1.0 and 3.0 s, central-transition selective $\pi/2$ pulse widths of 1.5 to 2.5 μs (which correspond to $\nu_1 = 83.3$ and 50 kHz, respectively). MAS NMR experiments employed spinning speed (ν_{rot}) ranging from 20.0 to 22.5 kHz. Additional experimental details are given in **Tables S4-S9**.

Spectral Simulations. Analytical simulations of ^{35}Cl SSNMR spectra were performed using the WSolids software package.⁷⁵ Numerical simulations of spinning sideband manifolds in ^{35}Cl MAS NMR spectra were generated using SIMPSON,⁷⁶ using 10 gamma angles and powder averaging over 4180 crystal orientations calculated using the Zaremba-Conroy-Wolfsberg (ZCW) method. The uncertainties in EFG and CS tensor parameters were estimated using bidirectional variation of parameters and comparison of experimental and simulated spectra.

Powder XRD. The purity and crystal structures of all samples were confirmed using powder XRD. Patterns were collected using a D8 DISCOVER X-ray diffractometer equipped with an Oxford Cryosystems 700 Cryostream Plus Cooler. A Cu-K α ($\lambda = 1.54056 \text{ \AA}$) radiation source with a Bruker AXS HI-STAR area detector running under the General Area Detector Diffraction Systems (GADDS) were used. Powder XRD patterns were simulated with the PowderCell software package.⁷⁷

Theoretical Calculations. First principles calculations of ³⁵Cl EFG and nuclear magnetic shielding (NMS) tensor parameters were conducted on the Shared Hierarchical Academic Research Computing Network (SHARCNET).⁷⁸ Euler angles were calculated using the EFGShield software program.⁷⁹ All calculations were performed on coordinates derived from reported crystal structures⁸⁰⁻⁹² using the CASTEP⁶⁶⁻⁶⁹ code in the Materials Studio 5.0 software suite which utilizes the gauge-including projector augmented wave algorithm (GIPAW)⁶⁶ for NMR calculations. Calculations utilized the generalized gradient approximation (GGA), revised Perdew, Burke and Ernzerhof (rPBE) functional with on-the-fly pseudopotentials, a k -point spacing of 0.08 \AA , and a plane wave basis set cut-off energy of 500 eV.⁹³ Due to the general unreliability of hydrogen atom positions determined from X-ray diffraction, all such positions were geometry optimized within the CASTEP software package prior to calculation of the NMR parameters.⁶⁶⁻⁶⁹ Full geometry optimizations, in which all atom positions in the unit cell were allowed to vary, were also completed for each structure, with the exception of DibU. Calculations of NMR tensor data for the DibU structure were not completed due to its large unit cell size and associated computational limitations. During each geometry optimization only the atomic positions were allowed to vary, the lattice parameters were fixed at all times.

Results and Discussion

First, a general overview of the plane-wave DFT calculations of ^{35}Cl NMR tensor parameters is given. Second, ^{35}Cl SSNMR spectra of HCl pharmaceuticals are presented, along with detailed discussion of the EFG and CS tensor parameters obtained from analytical simulations of the ^{35}Cl SSNMR spectra, and theoretically obtained ^{35}Cl EFG tensor orientations. In this section, the compounds are organized by the number of short $\text{H}\cdots\text{Cl}$ contacts, which we *arbitrarily* define as contacts having an $\text{H}\cdots\text{Cl}$ distance of less than 2.6 Å. This assignment is based on “back-of-the-envelope” EFG point charge calculations that suggest that the ^{35}Cl EFG tensor properties (i.e., parameters and tensor orientation) can be significantly affected by hydrogen atoms located ca. 2.6 Å or less from the ^{35}Cl nuclei. This upper cutoff of 2.6 Å is consistent with a range of $\text{H}\cdots\text{Cl}$ hydrogen bonds encountered in organic systems containing chlorine anions, as described by Desiraju and Steiner.⁹⁴ Finally, the application of ^{35}Cl SSNMR for the differentiation of pharmaceutical polymorphs for two different APIs is discussed.

All experimental and calculated ^{35}Cl EFG and CS tensor parameters, including the Euler angles that describe the relative orientations of these tensors, are listed in **Tables 1** and **2**. All HCl APIs are listed in **Tables 3**, **4** and **5** with their corresponding NMR parameters, C_Q , η_Q and δ_{iso} , and the type(s) and length(s) of each hydrogen-bond contact. We note that experimentally determined hydrogen positions are either approximated or unknown for all of these systems: hydrogen atom positions derived from XRD data are unreliable and there are no neutron structures available for these APIs. Hence, hydrogen positions approximated from refined crystal structures were geometry optimized utilizing CASTEP, and resulting structures were utilized for subsequent calculations of NMR tensor parameters. Accurate determinations of the EFG and CS tensor parameters were achieved by acquisition and simulation of static ^{35}Cl powder

patterns at both 21.1 T and 9.4 T. Data from previous ^{35}Cl SSNMR studies of similar HCl compounds are also included for comparison.

Plane-Wave DFT Calculations. Previous computational work on model clusters of HCl APIs demonstrated that restricted Hartree-Fock (RHF) molecular orbital (MO) calculations of ^{35}Cl EFG tensors are in relatively good agreement with corresponding experimental NMR data.⁵⁹ Conventional MO calculations, unlike their GIPAW/plane-wave counterparts, do not take into account the three-dimensional periodicity inherent in the crystal lattice of a solid. In order to emulate an extended array of atoms, a cluster approximation is used where the central Cl atom is chosen, a large cluster is constructed, and large functional “terminating” groups that are distant from the central Cl atom are replaced with hydrogen atoms or methyl groups. The accuracy of the calculation is dependent on the size of the cluster, and how well this cluster acts as an approximation of the extended periodic structure. The latter point is a very subjective one to judge, due to the large number of variables involved in such calculations that influence their agreement with experimentally obtained data (i.e., accurate hydrogen atom positions, long-range electrostatic interactions, appropriate positioning and identity of terminating groups, buildup of excess positive/negative charges, etc.). Furthermore, calculations on large clusters can be very computationally demanding, even with the use of locally dense basis sets. Hence, for this work, we opted to focus on plane-wave DFT computational methods, which exploit the periodicity of solids, and enable effects like long-range electrostatic interactions to be better taken into account.

In this study, plane-wave calculations of NMR interaction tensors were performed on model systems for all of the APIs, with the exception of Dibu (see the **Experimental** section for details). In all cases, initial molecular coordinates of the heavy (non-hydrogen) atoms were obtained from single-crystal X-ray structures.^{80, 82-86, 88, 90-92} As mentioned in the experimental

section of this paper, we have conducted extensive calculations of ^{35}Cl EFG tensors on two types of model systems (in most cases) for purposes of comparison: (i) *optimization of hydrogen positions*: fixed XRD coordinates were used for the heavy atoms and the hydrogen positions were geometry optimized and (ii) *full geometry optimization*: starting from the known X-ray structure, all atom positions in the unit cell were geometry optimized. A test set of calculations reveal that the values of C_Q for the hydrogen-optimized models are generally in good agreement with experiment, but better agreement is observed for the fully optimized models (**Figure S1**); hence, we restrict the remainder of our discussion to the latter.

The ^{35}Cl EFG tensor parameters associated with the fully geometry optimized model structures are included for comparison with experimental data in **Tables 1 and 2**. The agreement between experimental and theoretical absolute values of C_Q is good, with an R^2 value of 0.9118 (**Figure 1a**). However, the calculated values of C_Q are consistently larger than their corresponding experimental values, which is not unusual for such comparisons (this is reflected in the calculated slope in **Figure 1a**, which is less than 1.0). Interestingly, Bryce et al. reported that MO calculations utilizing hybrid DFT methods consistently overestimated the magnitude of C_Q , while those using RHF method resulted in underestimations.⁶⁰ The experimental and theoretical values of η_Q for the same set of systems are in poorer agreement by comparison ($R^2 = 0.630$, **Figure S1c**); however, this improves somewhat if Amin, the clear outlier in terms of η_Q values, is excluded ($R^2 = 0.6995$, **Figure 1b**). It is possible that the generally better agreement between experimental and theoretical values of C_Q , and poorer agreement for concomitant values of η_Q , stem from the fact that the former relies only upon the accurate calculation of a single component of the EFG tensor (V_{33}), while the latter depends upon the accurate calculation of the relative values of all three components (V_{11} , V_{22} , V_{33}).

There are two main factors that may play important roles in differentiating the experimentally measured and theoretically determined quadrupolar parameters. First, it is very clear that accurate knowledge of proton positions is crucial for the accurate determination of the EFG tensor parameters. If even one of the closely positioned hydrogen atoms is out of place, this can have a severe impact on the values of C_Q and η_Q , as well as the EFG tensor orientations. Second, it is quite possible that motional dynamics may play a role in averaging (or reducing/augmenting) some/all of the components of the EFG tensors, as discussed by Dracinsky and Hodgkinson, who examined the averaging of anisotropic chemical shift parameters via a combination of MD and DFT calculations.⁹⁵ In the cases of HCl salts of APIs and amino acids, such averaging effects are unlikely to arise from the motion of the chlorine anions themselves, but rather, from the motions of the local hydrogen atoms and their associated moieties.

It is worth noting that calculations of ^{35}Cl EFG tensors for multiple candidate structures, perhaps determined through simulated annealing methods, genetic algorithm methods, and the like,⁹⁶ would likely reveal improved matches between experimental and theoretical data, making this data useful for ab initio crystal structure determination. As mentioned above, it is the positions of the closest bound hydrogen atoms that are the most crucial determinants of the nature of the ^{35}Cl EFG tensors. For example, Emsley, Day and co-workers have utilized experimentally measured ^1H chemical shifts, crystal prediction methods and DFT chemical shift calculations to predict crystal structures of several small APIs;⁵¹ we anticipate that it will be possible to utilize EFG tensors in a similar fashion.

Unfortunately, the theoretical chlorine nuclear magnetic shielding (NMS) tensor parameters exhibit poor correlation with experimentally determined CS tensors, (see **Figure S2**), suggesting that plane-wave methods are inadequate for these systems. We have recently shown⁵⁴

that whereas some useful correlations are found between the ^{35}Cl EFG tensor parameters and the local chlorine anion structural environments, no similar trends have been found for the chlorine CS or NMS tensor parameters. Nonetheless, the unique sets of CS tensor parameters are very useful for spectral fingerprinting of the APIs. Therefore, for the remainder of this work, discussion of the results of these calculations focuses mainly upon the theoretically derived ^{35}Cl EFG parameters and tensor orientations.

Systems with one short H \cdots Cl contact: Adiphenine HCl (Adip), Buflomedil HCl (Bufl), Dicyclomine HCl (Dicy) and Trigonelline HCl (Trig). The crystal structures of Adip, Bufl, Dicy and Trig have a single chlorine site in their respective asymmetric units, each of which is involved in one H \cdots Cl contact of less than 2.6 Å (in fact, all single contacts are less than 2.03 Å, **Table 3**). The ^{35}Cl SSNMR spectra (**Figure 2**) are indicative of single chlorine sites, consistent with the crystal structures. Analytical simulations of the spectra, acquired at both 9.4 and 21.1 T, reveal ^{35}Cl EFG and CS tensor parameters that are similar to those of tetracaine HCl (Tetr) which also has a single Cl^- site (**Table 3**).⁵⁴ The only exception is the η_Q value for Dicy: for systems with one short H \cdots Cl contact, η_Q is typically close to zero (**Table 3**); however, in the case of Dicy, η_Q has an intermediate value of 0.45, indicating a non-axially symmetric ^{35}Cl EFG tensor. Of these four systems, Dicy is the only system where V_{11} and V_{22} are oriented in directions close to the directions of H \cdots Cl contacts of ca. 2.6 Å, which may account for the intermediate η_Q (in all other cases, V_{11} and V_{22} are not positioned near any short contacts).

We previously showed that for a small set of four one-contact HCl APIs, the absolute magnitude of C_Q increases with decreasing H \cdots Cl contact distance (**Table 3**).⁵⁴ With the addition of more samples to this dataset, it is apparent that there is not a clear relationship between C_Q and H \cdots Cl distance (**Figure S3**). The magnitudes of C_Q for Dicy and Bufl are equal,

within experimental error, owing to the fact that they each have one H \cdots Cl close contact from the same type of moiety (R₃NH⁺) and very similar H \cdots Cl contact distances (as best as we can tell from the X-ray structures, **Table 3**). It must be noted that one-contact systems typically have the largest absolute magnitudes of C_Q , as in the cases of trigonelline HCl ($C_Q = 7.50$ MHz) and aspartic acid HCl ($C_Q = 7.1$ MHz),⁹⁷ both of which have a single short H \cdots Cl contact involving a carboxylic acid moiety.

The theoretical ³⁵Cl EFG tensor orientations for one-contact HCl API's reveal that in each case, V_{33} , the largest component of the EFG tensor, is directed along, or near, the shortest H \cdots Cl close contact, as shown in **Figure 3**. The sign of C_Q is predicted to be negative for each of these systems (N.B., (i) in each case, the sign of V_{33} is predicted to be positive, and $C_Q = V_{33}eQ/h$ is negative, since Q is negative; and (ii) the sign of C_Q cannot be determined from NMR spectra of central transition patterns). Finally, the Euler angle β is predicted to be close to zero for all of these systems, indicating that the largest component of the EFG tensor, V_{33} , is almost coincident with the largest (most shielded) component of the NMS tensor, σ_{33} , in each case.

Systems with two short H \cdots Cl contacts: Ranitidine HCl (Rani), Dibucaine HCl (Dibu site 1), Scopolamine HCl (Scop), Mexiletine HCl site 1 (Mexi site 1) and Bromhexine HCl (Brom). The crystal structures of both Rani and Scop have single chlorine sites, each involved in two close H \cdots Cl contacts (**Table 3**). The crystal structures of Mexi and Dibu have two chlorine sites; for now, we discuss the two chlorine sites with two short contacts: Mexi site 1 and Dibu site 1. Mexi site 2 has four contacts and is discussed later. Dibu site 2, which is coordinated by a water molecule (i.e., a hydrate), is not discussed in the current work; hydrates and solvates will be the subject of a future study.

The ^{35}Cl SSNMR spectra of the first four compounds are shown in **Figure 4**. The values of C_Q for Rani, Dibu site 1 and Scop are generally smaller than those of the one-contact systems, and the values of η_Q are near unity (**Table 1**). Interestingly, the C_Q associated with Scop is much lower than the other systems involving two hydrogen contacts, and its δ_{iso} (0 ppm) is the lowest chemical shift of all of the HCl APIs studied to date; it is unique in this set in not having a single $\text{H}\cdots\text{Cl}$ near or less than ca. 2.0 Å. The C_Q value for site 1 is larger than that of Rani and Scop, and the value of η_Q is further from unity. The higher value of C_Q for Mexi site 1 likely results from the presence of an extremely short (< 2.0 Å) $\text{H}\cdots\text{Cl}$ contact absent in Rani, Scop, and perhaps for Dibu site 1 (we cannot comment definitively for Dibu, since plane-wave DFT geometry optimizations and associated EFG tensor calculations failed for this system).

In general, for the two-contact APIs discussed so far, the theoretical ^{35}Cl EFG tensors are oriented such that V_{33} is approximately perpendicular to the plane of the two closest $\text{H}\cdots\text{Cl}$ contacts (see **Figure 5** for the case of Scop and Rani; Mexi site 1, which has an intermediate value of η_Q , has a similar tensor orientation, and is discussed in the polymorphs section below). Interestingly, the signs of C_Q are predicted to be positive for all of these systems (i.e., V_{33} values are negative). In comparing the one- and two-contact systems, we make the preliminary observation that if V_{33} is aligned along or near the direction of the shortest contact, the sign of C_Q is negative (V_{33} positive), and if V_{33} is aligned approximately perpendicular to this direction, the sign of C_Q is positive (V_{33} negative). In other words, the EFGs are positive in the direction of the bonds, and negative in the directions perpendicular to the bonds.

Brom represents an interesting case that combines features of one- and two-contact systems. For Brom, the absolute value of C_Q is larger than expected for systems with two short $\text{H}\cdots\text{Cl}$ contacts. Additionally, the η_Q is close to zero, indicating an EFG tensor with almost axial

symmetry, further distinguishing itself from other two-contact systems (**Table 3, Figure 6**). These data suggest that the ^{35}Cl EFG tensor orientation is distinct in comparison to the other so-called two-contact systems, and should likely be similar to that of the one-contact systems. Indeed, ^{35}Cl EFG tensor calculations on Brom indicate that V_{33} is oriented near to the direction of the closest hydrogen contact ($\angle(V_{33}\text{-Cl-H}) = 16.14^\circ$), and V_{22} is approximately perpendicular to the plane formed by the two close contacts (**Figure 7**). The sign of C_Q is negative, which is consistent with the orientation of V_{33} near the direction of the shortest $\text{H}\cdots\text{Cl}$ contact; in fact, under our classification system based on arbitrary shortest contact distances, Brom would be better assigned to the group of the one-contact systems based on the similarity of their respective EFG tensor parameters. In this case, the positive V_{33} component simply has a larger absolute magnitude than the negative V_{22} . Hence, for all of the one- and two-contact systems, regardless of our arbitrary classifications based on numbers of contacts $< 2.6 \text{ \AA}$, values of V_{33} are positive along the directions of the shortest contacts and negative in perpendicular directions, with the relative absolute magnitudes and orientations of V_{22} and V_{33} determined by contact distances of the nearest hydrogen atoms. In the case of Brom, the orientation of V_{33} and increase in the absolute magnitude of C_Q result from the presence of a single, very short contact (i.e., typically ca. 2.0 \AA or less). This is consistent with our previous observations within a series of four HCl APIs.⁵⁴

Systems with three short $\text{H}\cdots\text{Cl}$ contacts: Alprenolol HCl (Alpr), Isoprenaline HCl (Isop), Acebutolol HCl (Aceb), Amantadine HCl (Aman) and Procainamide HCl (Proc).

The chloride anions in Alpr, Isop, Aceb, Aman and Proc are involved in three short hydrogen contacts (**Table 4**). We focus our discussion on the first four systems for now. The ^{35}Cl SSNMR spectra reveal central transition powder patterns corresponding to single chlorine sites

in each case (**Figure 8**). The chlorine anions in Alpr, Isop and Aceb are involved in three hydrogen contacts involving both NH and OH groups (**Table 4**), and all have similar values of C_Q and moderate to high values of η_Q . Notably, both Alpr and Isop have a single H \cdots Cl contact distance of ca. 2.05 Å and another of ca. 2.10 to 2.15 Å, perhaps account for their C_Q values which are slightly larger than that of Aceb. In addition, their shortest H \cdots Cl contacts involve different functional groups. Aman has a markedly lower value of C_Q by comparison; however, in Aman, the H \cdots Cl contacts involve RNH $_3^+$ moieties exclusively. The C_Q for Aman is comparable to that of Lcme (2.37 MHz), which also only has three short hydrogen contacts involving nitrogen-containing groups.⁵⁸ Therefore, it appears that the absolute value of C_Q is generally smaller if there are no short hydrogen contacts involving oxygen-containing moieties (similar trends are observed for two-contact systems).

In general, for these three-contact APIs, the theoretical ^{35}Cl EFG tensors are oriented such that V_{33} is not directed along or near the directions of the shortest contacts. In all cases, the signs of C_Q are predicted to be positive (i.e., V_{33} values are negative), consistent with observations made for the one- and two-contact systems above. The V_{11} and V_{22} components are sometimes oriented near short contacts, and sometimes between the directions of these contacts, never adopting orientations that could be said to be universal for all of these systems (see **Figure 9**). In the absence of one short contact, there are many longer-range EFGs that become noteworthy and influence the ^{35}Cl EFG tensors.

Simulations of the ^{35}Cl SSNMR spectra of Proc reveal a value of C_Q equal to 4.25 MHz (**Figure 10, Table 2**). The three short H \cdots Cl contacts involve only nitrogen-containing moieties, as in the cases of Lcme and Aman; however, the absolute value of C_Q of the former is much larger than those of the latter. The closest H \cdots Cl contact in Proc is shorter than those of Lcme

and Aman, which may account for the larger absolute value of C_Q and undoubtedly influences the EFG tensor orientation. The calculated ^{35}Cl EFG tensor orientation for Proc features V_{33} directed toward the shortest $\text{NH}\cdots\text{Cl}$ contact ($\angle(V_{33}\text{-Cl-H}) = 14.83^\circ$), V_{11} oriented towards the longest contact, and V_{22} nearly perpendicular to the approximate plane formed by the three $\text{H}\cdots\text{Cl}$ contacts (**Figure 11**). The sign of C_Q is predicted to be negative (i.e., V_{33} is positive), consistent with the presence of very short contacts (ca. 2.0 Å or less). As in the case of Brom, it seems that Proc is better classified as having a single short contact that dominates the nature and orientation of the ^{35}Cl EFG tensor.

Again, as in the case of the previously described systems, principal components of the EFG tensor that are large and positive are directed near the directions of short contacts, and those that are negative are directed perpendicular to the directions of these contacts. Hence, the EFG tensors are not dramatically varying in orientation from system to system; rather, the relative magnitudes of the largest positive and negative principal components are alternating as V_{33} and V_{22} , depending upon the relative distances of the shortest contacts. This data for all of the three-contact systems that have been studied with ^{35}Cl SSNMR implicates the contact distance (in particular, the presence of one very short contact) as one of the most important factors influencing the EFG tensor parameters and orientation, along with the nature of the surrounding moieties.

Systems with four or more short $\text{H}\cdots\text{Cl}$ contacts: Isoxsuprine HCl (Isox), Mexiletine HCl site 2 (Mexi site 2), Dopamine HCl (Dopa) and Aminoguanidine HCl (Amin). The structures of Isox and Mexi site 2 have four close $\text{H}\cdots\text{Cl}$ contacts, whereas Dopa and Amin have five and six $\text{H}\cdots\text{Cl}$ contacts, respectively (**Table 5**). There is a unique powder pattern in each of the ^{35}Cl SSNMR spectra corresponding to the single chlorine sites of Isox, Dopa and Amin

(**Figure 12**). The spectrum for Mexi, which features two unique patterns, is shown in **Figure 4**. For Isox, the C_Q is relatively large (5.50 MHz), likely owing to the mixture of OH and NH hydrogen bonding moieties, as discussed previously. Conversely, Mexi site 2 has a lower value of C_Q , due to the H \cdots Cl contacts involving only nitrogen-containing moieties. The tensor orientations for Isox and Mexi are discussed in the polymorph section of this work (vide infra).

The quadrupolar parameters of Dopa are similar to those of three-contact systems like Alpr and Isop, and the four-contact Treo,⁹⁷ all of which have multiple OH and NH contacts. In addition, the shortest H \cdots Cl contact for all of these systems is near 2.00 Å, presumably accounting for the large absolute magnitudes of C_Q in each case. The largest component of the EFG tensor, V_{33} , is directed toward the shortest H \cdots Cl contact ($\angle(V_{33}\text{-Cl-HO}) = 15.67^\circ$), similar to many of the HCl APIs with one very short H \cdots Cl contact and larger magnitudes of C_Q .⁵⁴ V_{22} is directed toward a different short hydrogen contact, and V_{11} bisects the angle formed by two of the five short hydrogen contacts, as shown in **Figure 13(a)**.

Of all of the APIs studied via ^{35}Cl SSNMR, Amin has the greatest number of short H \cdots Cl contacts with distances of less than 2.6 Å, as well as the lowest measured value of C_Q to date (the second smallest is that of Lcme, $C_Q = 2.37$ MHz, which has three $\text{RNH}_3^+\cdots\text{Cl}$ contacts).⁵⁸ The short H \cdots Cl contacts in Amin only involve nitrogen-containing moieties, and not surprisingly, the low magnitude of C_Q is similar to those for other systems that have multiple H \cdots Cl close contacts involving only NH containing moieties, such as Lcme,⁵⁸ Aman and Mexi site 2. There are six short H \cdots Cl contacts in Amin; however, unlike Dopa, there is no short contact with a distance less than 2.2 Å. Accordingly, calculations predict that V_{33} is not directed near a short H \cdots Cl contact, but rather, points into areas where there are no nearby hydrogen atoms (**Figure**

13(b)), with V_{11} and V_{22} approximately bisecting two H \cdots Cl close contacts. In addition, V_{33} is negative, meaning that the value of C_Q is positive, as expected.

A summary of correlations of chlorine environments and ^{35}Cl EFG tensor parameters. Considering the systems discussed above, there are several trends in the ^{35}Cl EFG tensor parameters that can be correlated to the structure of the local chlorine environment.

1. For chlorine anions with a single H \cdots Cl contact less than 2.6 Å or multiple H \cdots Cl contacts where one of the contacts is very short (ca. 2.0 Å or less), V_{33} is directed along or near the direction of the shortest contact. Also, the “horns” of the central transition pattern are normally well separated, which is indicative of values of η_Q close to zero, which signifies that the ^{35}Cl EFG tensors have near-axial symmetry (cluster and plane wave calculations are in agreement with this conclusion). The only exception to this is Dicy, which has V_{11} and V_{22} oriented near the directions of H \cdots Cl contacts slightly longer than 2.6 Å. In addition, the calculated value of C_Q is invariably negative (i.e., positive V_{33}), and the Euler angle β is close to zero. There does not seem to be a simple correlation between the H \cdots Cl distance and the absolute magnitude of C_Q , indicating that charges on the individual atoms involved in these contacts, and perhaps additional longer range interactions, must also make significant contributions to the ^{35}Cl EFGs (**Figure S3**).

2. In systems where the chlorine anion has two close hydrogen contacts less than 2.6 Å, the value of C_Q is generally lower than those observed for one-contact systems, and η_Q is typically high, approaching unity. The value of C_Q appears to be highly dependent on the geometric arrangement of the hydrogen donor moieties. In particular, the absolute magnitude of C_Q is found to be the largest in systems where one or both of the two contacts is/are very short (ca. 2.00 Å). The EFG tensor orientation is relatively consistent among all of these systems, with

one of V_{22} or V_{33} oriented near the shortest contact, and the other approximately perpendicular to the H-Cl-H plane. In cases where there is a single very short contact distance (ca. 2.0 Å or less), V_{33} is oriented near or along the direction of the shortest contact, akin to the one-contact systems.

3. For three H \cdots Cl contact systems, the lowest magnitudes of C_Q are found in systems with H \cdots Cl contacts involving only nitrogen-containing moieties. Higher magnitudes of C_Q occur in systems with mixed OH and NH moieties and/or at least one short H \cdots Cl distance less than 2.0 Å. This latter characteristic is shared in common with the two-contact systems. There is no “typical” orientation to be found, as for the one- and two-contact systems, since in the absence of a single short contact, the ^{35}Cl EFG tensor is influenced by a variety of EFGs with their origins in multiple directions.

4. For systems with four or more contacts, similar relationships as those described for three-contact systems are observed.

5. The sign of C_Q , which cannot be determined from direct observation of SSNMR spectra of quadrupolar nuclei, but can be obtained via theoretical calculations from EFG tensor parameters, is clearly related to two distinct possibilities for ^{35}Cl EFG tensor orientations. Regardless of the number of short H \cdots Cl contacts (i.e., less than 2.6 Å), if there is a single distinct short contact distance of ca. 2.0 Å or less, the principal component that is oriented along/near the direction of this contact is positive. For example, in Proc, Brom and Dopa, V_{33} is oriented near the direction of the shortest contact, and for all of these systems, the C_Q is predicted to be negative (i.e., V_{33} is positive and V_{22} is negative, with the latter not oriented near a short contact). However, in Alpr, Isop and Scop, V_{33} is directed perpendicular to the direction of the shortest contact, and the C_Q is predicted to be positive (i.e., V_{33} is negative, meaning the V_{22} , which is positive, is nearest to the shortest contact). C_Q is unvaryingly predicted to be positive

for systems with no short contacts and/or exclusively having NH moieties involved in close contacts less than 2.6 Å.

6. Finally, for all of the APIs, there are no obvious trends that correlate the CS tensor parameters to the local structures of the chlorine anion environments. However, we strongly emphasize that accurate determination of the CS tensor parameters is crucial for the differentiation and fingerprinting of different HCl species, and proves to be extremely important for polymorph recognition (*vide infra*).

Application to polymorphism in HCl pharmaceuticals. In this section, we examine the application of ^{35}Cl SSNMR for the identification, differentiation and fingerprinting of structural polymorphs. We examine two sets of systems from the series of APIs discussed above, Isox and Mexi. The complete listing of experimental and theoretical ^{35}Cl SSNMR parameters is given in **Table 6**. It is noted that crystal structures are available for most of these systems and their polymorphs. Hence, newly discovered polymorphs are not being identified herein; rather, we are trying to determine what information is available from the ^{35}Cl SSNMR spectra and the concomitant DFT calculations, and how this information can be used either independently or in concert with data from other characterization methods, including ^{13}C SSNMR spectroscopy and X-ray diffraction experiments.

Isoxsuprine HCl (Isox). The crystal structure of Isox has one chlorine atom in the asymmetric unit that is involved in four short hydrogen contacts (two $\text{Cl}\cdots\text{HO}$ and two $\text{Cl}\cdots\text{HN}$, **Table 7**). The ^{35}Cl SSNMR spectra of Isox are shown in **Figure 14(a)**. The C_Q is relatively large (5.50 MHz) for a system with four $\text{H}\cdots\text{Cl}$ close contacts, likely owing to the mixture of OH and NH hydrogen bond donors, as discussed previously. IsoxI is a polymorph of Isox which is generated by recrystallization from methanol (see Supporting Information for experimental

details).⁸⁶ IsoxI has two distinct chlorine sites, both involved in four short H \cdots Cl contacts from NH- and OH-type moieties (**Table 7**). The static ^{35}Cl SSNMR spectrum (9.4 T) of IsoxI clearly reveals two overlapping chlorine powder patterns (**Figure 14(b)**). Site 1 has a broader central transition pattern, a larger C_Q , a slightly higher η_Q , and a smaller span in comparison to site 2. Site 2 and the lone Cl^- site in Isox, which have similar four-contact environments, also share very similar quadrupolar parameters. This could lead one to surmise that the IsoxI sample is simply a mixture of two different crystalline samples (i.e., in the absence of single crystal XRD data). However, there are two pieces of evidence that prove that this is not the case: (i) the CS tensor parameters are very different, with the former having much larger span and distinctly lower isotropic chemical shift, and (ii) the pXRD patterns for each sample are completely distinct (**Figure S4**). This highlights, especially in light of the CS tensor data, how ^{35}Cl SSNMR can be utilized to differentiate and fingerprint polymorphs, either as a standalone or complementary technique.

The calculated ^{35}Cl EFG and NMS tensor parameters, obtained after full geometry optimization of the structures, are given in **Table 6** for Isox and IsoxI sites 1 and 2. In Isox, V_{33} is oriented such that it is approximately perpendicular to the pseudo-plane formed by the four close H \cdots Cl contacts, whereas V_{11} and V_{22} are directed near two of the four close hydrogen contacts ($(\angle(V_{11}\text{-Cl-H}) = 6.66^\circ, \angle(V_{22}\text{-Cl-H}) = 15.80^\circ)$), as depicted in **Figure 15(a)**. For IsoxI site 1, V_{33} is approximately perpendicular to the plane formed by the four close hydrogen contacts, and V_{22} and V_{11} approximately bisect two of the four short hydrogen contacts, as shown in **Figure 15(b)**. IsoxI site 2 has a similar EFG tensor orientation to that of Isox (**Figure 15(c)**). The $^1\text{H} \rightarrow ^{13}\text{C}$ VACP/MAS NMR spectra of Isox and IsoxI (**Figure S5**) display clear differences in the aromatic region of the spectrum, allowing for the accurate fingerprinting of these

polymorphs, provided that identical experimental conditions are met (i.e., contact times, recycle delays, etc.).^{32, 98-100} Although the pXRD patterns (**Figure S4**) and the $^1\text{H} \rightarrow ^{13}\text{C}$ VACP SSNMR spectra (**Figure S5**) are distinct for those of Isox and IsoxI, they offer little information (the latter in particular) regarding the differences in molecular-level structure between the polymorphs. In particular, it is not trivial to determine the number of crystallographically distinct chlorine sites from these data sets, together or independently; knowledge of this number can of course aid in the assignment/determination of the space group, and perhaps even in the eventual structural determination via Rietveld methods.

Mexiletine HCl. Of the six known polymorphs of Mexi, there is currently only one known crystal structure.¹⁰¹ Comparison of the simulated pXRD pattern for this crystal structure to the pattern measured in our laboratory reveals that the crystal structure corresponds to that reported by Sivy *et al.* (**Figure S6**).⁹¹ The crystal structure of Mexi has two chlorine sites: site 1 has two $\text{NH}\cdots\text{Cl}$ contacts, while site 2 has four $\text{NH}\cdots\text{Cl}$ contacts (**Table 7**). ^{35}Cl SSNMR spectra of Mexi (**Figure 16(a)**) reveal two distinct powder patterns corresponding to the crystallographically distinct chlorine sites. The pattern with the larger C_Q is readily assigned to site 1, since the $\text{NH}\cdots\text{Cl}$ contacts are very short in comparison to those of site 2 (this assignment is borne out by calculations, *vide infra*). Site 1 also has a lower isotropic chemical shift and distinct skew in comparison to site 2.

We have generated two polymorphs of Mexiletine HCl: MexiII and MexiIII (see **Supporting Information** for experimental details). There are currently no known crystal structures for these two polymorphs; however, pXRD patterns of these samples are distinct from each other and that of Mexi (**Figure S6**).

The ^{35}Cl SSNMR spectra of MexiI are shown in **Figure 16(b)** (see **Figure S7** for expanded views), and are strikingly different from those of Mexi (notably, in their breadths). The ^{35}Cl MAS NMR spectrum at 21.1 T (**Figure 16(b)**) does not display any spinning sidebands, due to a combination of a small C_Q and a small Ω . Further inspection of the spectrum reveals an increased intensity in the low frequency horn and a decreased intensity in the high frequency horn, as well as a characteristic ‘tail’ occurring to low frequency, which may indicate some degree of long-range disorder. The low value of C_Q (1.99 MHz) for MexiI gives rise to a number of insights: (i) there is no short contact distance of ca. 2.0 Å or less; (ii) there are likely not any oxygen-containing moieties involved in hydrogen bonding, since low values of C_Q measured in such systems are associated with three or more short contacts involving only $\text{NH}\cdots\text{Cl}$ interactions (e.g., Aman, Lcme and Amin).

The ^{35}Cl static powder pattern of MexiI at 21.1 T (**Figure 16(b)**) is relatively featureless, and clearly does not display any of the usual features associated with a central transition powder pattern of a half-integer spin quadrupolar nucleus. However, the same pattern at 9.4 T is dominated by the second-order quadrupolar interaction, displaying clearly recognizable features. The magnitudes of C_Q and Ω are small and comparable (when assessed in Hz), with the quadrupolar interaction dominating the low field spectrum, and the chlorine CSA dominating the high field spectrum (since the breadth of the central transition pattern scales as the reciprocal of the field strength for the former, and is proportional to the field strength for the latter). We note that one can observe some of the effects of CSA in the 9.4 T spectrum, manifested as a splitting of one of the discontinuities (**Figure S7**).

The broad and featureless ^{35}Cl SSNMR pattern of MexiII (9.4 T) is even more surprising, bearing no resemblance to a conventional second-order quadrupolar powder pattern (**Figure 17**).

Hence, accurate determination of its ^{35}Cl NMR parameters via analytical simulation is not possible. The pattern appears to be indicative of a chlorine site of high spherical symmetry and negligible quadrupolar interaction; there may also be some degree of local disorder at this site. The pXRD pattern of MexiII (**Figure S6(c)**) has very sharp peaks indicative of long-range ordering (crystallinity), indicating that the sample cannot be completely amorphous; however, this data does not reveal if the chlorine anion is possibly contained within a separate amorphous phase. Given this possibility, it is probably prudent to simply classify MexiII as a separate solid form of Mexi. Further structural characterization of this polymorph, and the potential investigation of chlorine anion dynamics, was subverted by the thermodynamic instability of the polymorph (it reverted back to Mexi after only 6 hours). In particular, ^{35}Cl SSNMR spectra could not be acquired offsite at 21.1 T at the National High Magnetic Field Laboratory in Tallahassee, FL. We intend to commit future time and experiments to preparing the samples on site so that experiments can be conducted within the appropriate time frame – a full multi-field, VT study is beyond the scope of the current manuscript.

The calculated chlorine EFG and NMS tensor parameters, obtained after full geometry optimization of the structure, are given in **Table 6** for Mexi. For site 1, V_{33} is approximately perpendicular to the plane formed by the two close hydrogen contacts and V_{22} is directed near a short $\text{H}\cdots\text{Cl}$ contact (V_{11} is not), perhaps accounting for the moderate value of η_Q (**Figure 18(a)**). For Mexi site 2, V_{11} approximately bisects two of the four $\text{H}\cdots\text{Cl}$ contacts and V_{22} is directed towards one of the close H contacts (**Figure 18(b)**). As there are currently no crystal structures available for MexiI and MexiII, it is not possible at this time to calculate their EFG and NMS tensor parameters. Techniques capable of predicting new phases and structures have been developed, which may show promise in predicting unknown crystal structures for HCl

pharmaceutical polymorphs; for example, the *ab initio* Random Structure Searching (AIRSS) algorithm may prove very useful in the future,^{51, 102-104} along with numerous other methods designed for predicting solid-state structures from first principles.^{96, 105, 106}

As for Isox, the pXRD patterns and ³⁵Cl SSNMR spectra clearly differentiate the polymorphic forms of Mexi. The ¹³C SSNMR spectra are very similar (**Figure S8**), perhaps providing just enough information to fingerprint the individual polymorphs. However, limited insight into specific structural differences is available from these spectra. The ³⁵Cl EFG tensor parameters provide insight into both the number and nature of the Cl⁻ environments, as well as local hydrogen bonding interactions. This data, in conjunction with the information obtained using other methods, should prove useful in refinement of crystal structures, as well as rapid and precise fingerprinting and differentiation of polymorphs.

Conclusions

HCl APIs have been studied via ^{35}Cl SSNMR spectroscopy at 9.4 T and 21.1 T. Some general relationships between the quadrupolar parameters and the nature of $\text{H}\cdots\text{Cl}$ bonding have been established. In the case of systems with one contact with an $\text{H}\cdots\text{Cl}$ distance less than 2.6 Å, the nature of the ^{35}Cl EFG tensor is largely dependent on this contact. The absolute magnitude of C_Q is highly dependent upon the distance of the shortest contact, and values of η_Q are generally found to be close to zero (i.e., ^{35}Cl EFG tensors have near-axial symmetry). This implies that V_{33} must be directed along or near the direction of the shortest $\text{H}\cdots\text{Cl}$ contact. For systems with two contacts, the absolute magnitude of C_Q is generally lower than those of the one-contact systems, and the values of η_Q are closer to unity, indicating that the ^{35}Cl EFG tensor is not axially symmetric, and V_{33} is not oriented near the shortest contacts. For systems with three or more contacts, the values of η_Q range from moderate to near unity. In addition, the absolute magnitude of C_Q is larger for systems with a mix of NH and OH hydrogen bonding moieties, and smaller for systems having only nitrogen-containing hydrogen bonding moieties. Finally, regardless of the number of short contacts, if there is a single short $\text{H}\cdots\text{Cl}$ contact of ca. 2.0 Å or less, the absolute magnitude of C_Q is large and the value of η_Q is closer to zero, meaning that such short contacts almost completely determine the nature of the ^{35}Cl EFG tensors. Values of C_Q garnered from plane-wave DFT calculations are generally in good agreement with experimentally determined parameters; the best agreement is found for model systems in which all of the atoms (heavy atoms as well as hydrogen atoms) have been geometry optimized. However, poorer correlation is consistently observed between calculated and experimental values of η_Q , as well as the ^{35}Cl NMS tensor parameters. This may be due to a number of factors, including incorrectly optimized hydrogen positions (which have enormous impact on the

^{35}Cl EFG tensor parameters, in particular), and perhaps limitations in the chlorine atom pseudopotentials.

Calculations also reveal that the ^{35}Cl EFG tensor orientations and the signs of C_Q are highly dependent on the number and nature of the short contacts. For systems with a single short $\text{H}\cdots\text{Cl}$ contact of less than 2.6 Å, or multiple contact systems with a single short contact of ca. 2.0 Å or less, V_{33} is always predicted to be oriented near or along the direction of the shortest contact, and to have a positive sign (meaning that C_Q is negative). For other multiple contact systems, V_{33} is normally predicted to be oriented perpendicular to planes of two or three atoms involved in the shortest $\text{H}\cdots\text{Cl}$ contacts, and to have a negative sign (C_Q is positive). Hence, positive and negative EFGs are consistently associated with EFG tensor orientations in which V_{33} is oriented approximately along or perpendicular to the shortest $\text{H}\cdots\text{Cl}$ contact, respectively.

We have also demonstrated that ^{35}Cl SSNMR is an excellent spectroscopic technique for the differentiation of HCl pharmaceutical polymorphs: multiple sites are easily identified, and each polymorph has a unique spectral “fingerprint” that is associated with eight unique parameters. In order to obtain an accurate EFG and CS tensor parameters, it is strongly recommended that spectra be acquired at two distinct magnetic field strengths. Very high fields like 18.8 or 21.1 T are not necessary for routine investigations, but very useful for the potential examination of low concentrations of APIs in dosage forms. ^{35}Cl SSNMR spectra can be acquired rapidly with respect to standard ^{13}C SSNMR spectra acquired under CP/MAS conditions, and provide unambiguous differentiation of samples. Differentiation of HCl polymorphs that are non-crystalline or amorphous, or contained within samples with no longer-range order, is feasible using ^{35}Cl SSNMR, a clear advantage over pXRD methods. In particular, investigation of dosage forms (i.e., pills, capsules, tablets) is particularly attractive, since both

pXRD patterns and ^{13}C SSNMR spectra generally have interfering signals from the excipient matrices (e.g., cellulose and other binders).

We believe this work establishes ^{35}Cl SSNMR as both a standalone and complementary technique for the identification, differentiation and fingerprinting of polymorphs of HCl pharmaceuticals. This work also initiates the construction of a database of ^{35}Cl SSNMR data for HCl pharmaceuticals, which may find use with new computational routines applied in the emerging field of NMR crystallography. Currently, chemical shift data (e.g., ^{13}C , ^1H) are being applied for structural refinement; we see no reason that ^{35}Cl NMR data cannot also play a major role in this field. Finally, given the rapidity with which the NMR spectra can be acquired, we believe that the methods outlined may find general use in the pharmaceutical industry as a method of characterizing HCl APIs and screening their associated polymorphs.

Acknowledgements

R.W.S. thanks NSERC for funding this research in the form of a Discovery Grant and Discovery Accelerator Supplement. R.W.S. is also grateful for an Early Researcher Award from the Ontario Ministry of Research and Innovation. HH and MH thank the Ontario Ministry of Research and Innovation for Ontario Graduate Scholarships, and AMN thanks NSERC for Undergraduate Student Research Scholarships and the University of Windsor for the Outstanding Scholars Award in Chemistry. We are also grateful for the funding of the Laboratories for Solid-State Characterization at the University of Windsor from the Canadian Foundation for Innovation, the Ontario Innovation Trust, and the University of Windsor. This work was made possible, in part, by the facilities of the Shared Hierarchical Academic Research Computing Network (SHARCNET: www.sharcnet.ca). We are also grateful to Dr. Karen Johnston for assistance with the CASTEP calculations. ZG, IH and RF, and the work performed at the National High Magnetic Field Laboratory, are supported by the National Science Foundation Cooperative Agreement DMR-0084173 and the State of Florida.

Supporting Information Available: Details on NMR acquisition parameters, polymorph generation, DFT calculation data, pXRD patterns, and ^{13}C NMR spectra are provided.

References

1. M. Geppi, G. Mollica, S. Borsacchi and C. A. Veracini, *Appl. Spectrosc. Rev.*, 2008, **43**, 202.
2. S. Lohani and D. J. W. Grant, *Polymorphism*, 2006, 21.
3. R. Hilfiker and Editor, *Polymorphism: In the Pharmaceutical Industry*, 2006.
4. S. P. F. Miller, A. S. Raw and L. X. Yu, *Polymorphism*, 2006, 385.
5. S. M. Reutzel-Edens, *Curr. Opin. Drug Discovery Dev.*, 2006, **9**, 806.
6. D. Singhal and W. Curatolo, *Adv. Drug Del. Rev.*, 2004, **56**, 335.
7. T. L. Threlfall, *Analyst*, 1995, **120**, 2435.
8. H. G. Brittain and D. J. W. Grant, *Polymorphism in Pharmaceutical Solids*, Marcel Dekker, New York, 1999.
9. J. K. Halebian and W. McCrone, *J. Pharm. Sci.*, 1969, **58**, 911.
10. P. H. Karpinski, *Chem. Eng. Technol.*, 2006, **29**, 233.
11. A. Llinas, K. J. Box, J. C. Burley, R. C. Glen and J. M. Goodman, *J. Appl. Crystallogr.*, 2007, **40**, 379.
12. D. Giron, *J. Therm. Anal. Calorim.*, 2003, **73**, 441.
13. S. R. Byrn, R. R. Pfeiffer, G. Stephenson, D. J. W. Grant and W. B. Gleason, *Chem. Mater.*, 1994, **6**, 1148.
14. D. Giron, *J. Therm. Anal. Calorim.*, 2001, **64**, 37.
15. D. Giron, *Am. Pharm. Rev.*, 2005, **8**, 72.
16. D. Giron, *Am. Pharm. Rev.*, 2005, **8**, 32.
17. D. Giron, *Pharmacokinetic Profiling in Drug Research: Biological, Physicochemical, and Computational Strategies, [LogP2004, Lipophilicity Symposium], 3rd, Zurich*, 2006, 307.
18. M. Maiwald, *Am. Pharm. Rev.*, 2006, **9**, 95.
19. B. E. Padden, M. T. Zell, Z. Dong, S. A. Schroeder, D. J. W. Grant and E. J. Munson, *Anal. Chem.*, 1999, **71**, 3325.
20. M. T. Zell, B. E. Padden, D. J. W. Grant, S. A. Schroeder, K. L. Wachholder, I. Prakash and E. J. Munson, *Tetrahedron*, 2000, **56**, 6603.
21. G. E. Martin and D. Sunseri, *J. Pharm. Biomed. Anal.*, 2011, **55**, 895.
22. V. V. Podgorskii, A. S. Mikhalev and G. A. Kalabin, *Pharm. Chem. J.*, 2011, **45**, 194.
23. Q. D. Zang, D. A. Keire, L. F. Buhse, R. D. Wood, D. P. Mital, S. Haque, S. Srinivasan, C. M. V. Moore, M. Nasr, A. Al-Hakim, M. L. Trehy and W. J. Welsh, *Anal. Bioanal. Chem.*, 2011, **401**, 939.
24. R. T. Berendt, D. M. Sperger, E. J. Munson and P. K. Isbester, *Trends Anal. Chem.*, 2006, **25**, 977.
25. R. K. Harris, *Analyst*, 2006, **131**, 351.
26. R. K. Harris, *J. Pharm. Pharmacol.*, 2007, **59**, 225.
27. U. Holzgrabe, *Prog. Nucl. Magn. Reson. Spectrosc.*, 2010, **57**, 229.
28. U. Holzgrabe, R. Deubner, C. Schollmayer and B. Waibel, *J. Pharm. Biomed. Anal.*, 2005, **38**, 806.
29. U. Holzgrabe, B. W. K. Diehl and I. Wawer, *J. Pharm. Biomed. Anal.*, 1998, **17**, 557.
30. M. Malet-Martino and U. Holzgrabe, *J. Pharm. Biomed. Anal.*, 2011, **55**, 1.
31. P. Gao, *Pharm. Res.*, 1996, **13**, 1095.
32. Y. G. Linck, A. K. Chattah, R. Graf, C. B. Romanuk, M. E. Olivera, R. H. Manzo, G. A. Monti and H. W. Spiess, *Phys. Chem. Chem. Phys.*, 2011, **13**, 6590.
33. T. J. Park, D. H. Ko, Y. J. Kim and Y. Kim, *Bull. Korean Chem. Soc.*, 2009, **30**, 2007.

34. T. N. Pham, C. J. Day, A. J. Edwards, H. R. Wood, I. R. Lynch, S. A. Watson, A. S. Z. Bretonnet and F. G. Vogt, *J. Pharm. Biomed. Anal.*, 2011, **54**, 401.
35. V. V. Terskikh, S. J. Lang, P. G. Gordon, G. D. Enright and J. A. Ripmeester, *Magn. Reson. Chem.*, 2009, **47**, 398.
36. T. Virtanen and S. L. Maunu, *Int. J. Pharm.*, 2010, **394**, 18.
37. N. Zumbulyadis, B. Antalek, W. Windig, R. P. Scaringe, A. M. Lanzafame, T. Blanton and M. Helber, *J. Am. Chem. Soc.*, 1999, **121**, 11554.
38. K. M. N. Burgess, F. A. Perras, A. Lebrun, E. Messner-Henning, I. Korobkov and D. L. Bryce, *J. Pharm. Sci.*, 2012, **101**, 2930.
39. V. Chupin, A. I. P. M. De Kroon and B. De Kruijff, *J. Am. Chem. Soc.*, 2004, **126**, 13816.
40. J. M. Griffin, M. R. Dave and B. P. Steven, *Angew. Chem. Int. Ed.*, 2007, **46**, 8036.
41. Z. J. Li, Y. Abramov, J. Bordner, J. Leonard, A. Medek and A. V. Trask, *J. Am. Chem. Soc.*, 2006, **128**, 8199.
42. E. D. L. Smith, R. B. Hammond, M. J. Jones, K. J. Roberts, J. B. O. Mitchell, S. L. Price, R. K. Harris, D. C. Apperley, J. C. Cherryman and R. Docherty, *J. Phys. Chem. B*, 2001, **105**, 5818.
43. F. G. Vogt, J. Brum, L. M. Katrincic, A. Flach, J. M. Socha, R. M. Goodman and R. C. Haltiwanger, *Cryst. Growth Des.*, 2006, **6**, 2333.
44. I. Wawer, M. Pisklak and Z. Chilmonczyk, *J. Pharm. Biomed. Anal.*, 2005, **38**, 865.
45. R. M. Wenslow, *Drug Dev. Ind. Pharm.*, 2002, **28**, 555.
46. K. M. Mao, J. L. Rapp, J. W. Wiench and M. Pruski, in *Electron Crystallography for Materials Research and Quantitative Characterization of Nanostructured Materials*, eds. P. Moeck, S. Hovmoller, S. Nicolopoulos, S. Rouvimov, V. Petkov, M. Gateshki and P. Fraundorf, Editon edn., 2009, vol. 1184, pp. 175.
47. P. A. Tishmack, D. E. Bugay and S. R. Byrn, *J. Pharm. Sci.*, 2003, **92**, 441.
48. R. K. Harris, S. Cadars, L. Emsley, J. R. Yates, C. J. Pickard, R. K. R. Jetti and U. J. Griesser, *Phys. Chem. Chem. Phys.*, 2007, **9**, 360.
49. N. Mifsud, B. Elena, C. J. Pickard, A. Lesage and L. Emsley, *Phys. Chem. Chem. Phys.*, 2006, **8**, 3418.
50. E. Salager, R. S. Stein, C. J. Pickard, B. Elena and L. Emsley, *Phys. Chem. Chem. Phys.*, 2009, **11**, 2610.
51. M. Baias, C. M. Widdifield, J. N. Dumez, H. P. G. Thompson, T. G. Cooper, E. Salager, S. Bassil, R. S. Stein, A. Lesage, G. M. Day and L. Emsley, *Phys. Chem. Chem. Phys.*, 2013, **15**, 8069.
52. L. D. B. Bighley, S. M.; Monkhouse, D. C., in *Encyclopedia of Pharmaceutical Technology*, ed. J. B. Swarbrick, J. C., Marcel Dekker, Editon edn., 1995, vol. 13, pp. 453.
53. C. C. Council, *The Benefits of Chlorine Chemistry in Pharmaceuticals*, Global Insights, Lexington, 2006.
54. H. Hamaed, J. M. Pawlowski, B. F. T. Cooper, R. Fu, S. H. Eichhorn and R. W. Schurko, *J. Am. Chem. Soc.*, 2008, **130**, 11056.
55. R. K. Harris, E. D. Becker, S. M. Cabral De Menezes, R. Goodfellow and P. Granger, *Concepts Magn. Reson.*, 2002, **14**, 326.
56. P. Pyykko, *Mol. Phys.*, 2001, **99**, 1617.
57. J. L. Dye, A. S. Ellaboudy and J. Kim, *Solid State NMR of Quadrupolar Nuclei*, Marcel Dekker, Inc., New York, 1991.
58. D. L. Bryce, M. Gee and R. E. Wasylshen, *J. Phys. Chem. A*, 2001, **105**, 10413.
59. D. L. Bryce and G. D. Sward, *J. Phys. Chem. B*, 2006, **110**, 26461.

60. D. L. Bryce, G. D. Sward and S. Adiga, *J. Am. Chem. Soc.*, 2006, **128**, 2121.
61. D. L. Bryce and E. B. Bultz, *Chem. Eur. J.*, 2007, **13**, 4786.
62. R. P. Chapman, C. M. Widdifield and D. L. Bryce, *Prog. Nucl. Magn. Reson. Spectrosc.*, 2009, **55**, 215.
63. C. M. Widdifield, R. P. Chapman and D. L. Bryce, *Annual Reports on NMR Spectroscopy*, 2009, **66**, 195.
64. D. L. Bryce and G. D. Sward, *Magn. Reson. Chem.*, 2006, **44**, 409.
65. F. A. Perras, Bryce, D.L., *Angewandte Communications*, 2012, **51**, 4227.
66. S. J. Clark, M. D. Segall, C. J. Pickard, P. J. Hasnip, M. J. Probert, K. Refson and M. C. Payne, *Z. Kristallogr.*, 2005, **220**, 567.
67. C. J. Pickard and F. Mauri, *Phys. Rev. B.*, 2001, **63**.
68. M. Profeta, F. Mauri and C. J. Pickard, *J. Am. Chem. Soc.*, 2003, **125**, 541.
69. J. R. Yates, C. J. Pickard and F. Mauri, *Phys. Rev. B.*, 2007, **76**.
70. D. Massiot, I. Farnan, N. Gautier, D. Trumeau, A. Trokiner and J. P. Coutures, *Solid State Nucl. Magn. Reson.*, 1995, **4**, 241.
71. A. Medek, V. Frydman and L. Frydman, *J. Phys. Chem. A*, 1999, **103**, 4830.
72. G. Metz, X. L. Wu and S. O. Smith, *J. Magn. Reson., Ser A*, 1994, **110**, 219.
73. A. E. Bennett, C. M. Rienstra, M. Auger, K. V. Lakshmi and R. G. Griffin, *J. Chem. Phys.*, 1995, **103**, 6951.
74. P. L. Gor'kov, E. Y. Chekmenev, C. Li, M. Cotten, J. J. Buffy, N. J. Traaseth, G. Veglia and W. W. Brey, *J. Magn. Reson.*, 2007, **185**, 77.
75. K. Eichele and R. E. Wasylishen, WSolids1: Solid-State NMR Spectrum Simulation, version 1.17.30, University of Tübingen, Tübingen, Germany, 2001
76. M. Bak, J. T. Rasmussen and N. C. Nielsen, *J. Magn. Reson.*, 2000, **147**, 296.
77. W. Kraus and G. Nolze, PowderCell for Windows, Berlin, Germany, 2000
78. This work was made possible by the facilities of the Shared Hierarchical Academic Research Computing Network (SHARCNET: <http://www.sharcnet.ca>).
79. S. Adiga, D. Aebi and D. L. Bryce, *Can. J. Chem.*, 2007, **85**, 496.
80. Y. Barrans, M. Cotrait and Dangouma.J, *Acta Crystallogr., Sect. B: Struct. Sci.*, 1973, **B 29**, 1264.
81. P. Chananont and T. A. Hamor, *Acta Crystallogr., Sect. B: Struct. Sci.*, 1981, **37**, 1878.
82. J. Giesecke, *Acta Crystallogr., Sect. B: Struct. Sci.*, 1980, **36**, 178.
83. R. Glaser, D. Shiftan and M. Drouin, *Can. J. Chem.*, 2000, **78**, 212.
84. R. Kingsfordadaboh, E. Hayashi, M. Haisa and S. Kashino, *Bull. Chem. Soc. Jpn.*, 1993, **66**, 2883.
85. C. H. J. Koo, Y. J.; Lee, S. W., *Arch. Pharm. Res.*, 1984, **7**, 115.
86. J. M. Leger, A. Carpy and J. C. Colleter, *Acta Crystallogr., Sect. B: Struct. Sci.*, 1981, **37**, 1927.
87. J. M. Leger, M. Goursolle and A. Carpy, *Cryst.Struct.Commun.*, 1981, **10**, 1365.
88. O. M. Peeters, N. M. Blaton, C. J. Deranter, O. Denisoff and L. Molle, *Cryst.Struct.Commun.*, 1980, **9**, 851.
89. R. Prewo and J. J. Stezowski, *J. Am. Chem. Soc.*, 1980, **102**, 7015.
90. A. E. Shvelashvili, G. V. Tsintsadze and E. B. Miminoshvili, *Zh. Neorg. Khim.*, 1996, **41**, 1851.
91. J. Sivy, V. Kettmann and E. Fresova, *Acta Crystallogr., Sect. C: Cryst. Struct. Commun.*, 1991, **C47**, 2695.

92. H. S. Yathirajan, B. Nagaraj, R. S. Narasegowda, P. Nagaraja and M. Bolte, *Acta Crystallogr., Sect. E: Struct. Rep. Online*, 2004, **E60**, o2228.
93. J. P. Perdew, K. Burke and M. Ernzerhof, *Phys. Rev. Lett.*, 1996, **77**, 3865.
94. G. Desiraju and T. Steiner, *The Weak Hydrogen Bond in Structural Chemistry and Biology*, Oxford University Press, Inc., New York, 1999.
95. M. Dracinsky and P. Hodgkinson, *Crystengcomm*, 2013, **15**, 8705.
96. S. M. Woodley and R. Catlow, *Nat. Mater.*, 2008, **7**, 937.
97. R. P. Chapman and D. L. Bryce, *Phys. Chem. Chem. Phys.*, 2007, **9**, 6219.
98. P. A. Beckmann, K. S. Burbank, K. M. Clemo, E. N. Slonaker, K. Averill, C. Dybowski, J. S. Figueroa, A. Glatfelter, S. Koch, L. M. Liable-Sands and A. L. Rheingold, *J. Chem. Phys.*, 2000, **113**, 1958.
99. W. Liu, W. D. Wang, W. Wang, S. Bai and C. Dybowski, *J. Phys. Chem. B*, 2010, **114**, 16641.
100. W. D. Wang, X. Gao, M. Strohmeier, W. Wang, S. Bai and C. Dybowski, *The Journal of Physical Chemistry B*, 2012.
101. A. Kiss and J. Repasi, *Analyst*, 1993, **118**, 661.
102. B. D. Malone and M. L. Cohen, *Phys. Rev. B.*, 2012, **85**.
103. A. J. Morris, C. P. Grey, R. J. Needs and C. J. Pickard, *Phys. Rev. B.*, 2011, **84**.
104. C. J. Pickard and R. J. Needs, *J. Phys.-Condes. Matter*, 2011, **23**.
105. G. Rossi and R. Ferrando, *J. Phys.-Condes. Matter*, 2009, **21**.
106. J. C. Schon, K. Doll and M. Jansen, *Phys. Status Solidi B-Basic Solid State Phys.*, 2010, **247**, 23.

Figure Captions

Scheme 1. Schematic representations of (a) adiphenine HCl (Adip), (b) buflomedil HCl (Bufl), (c) dicyclomine HCl (Dicy), (d) trigonelline HCl (Trig), (e) ranitidine HCl (Rani), (f) dibucaine HCl (Dibu), (g) scopolamine HCl (Scop), (h) mexiletine HCl (Mexi), (i) bromhexine HCl (Brom), (j) alprenolol HCl (Alpr), (k) isoprenaline HCl (Isop), (l) acebutolol HCl (Aceb), (m) amantadine HCl (Aman), (n) procainamide HCl (Proc), (o) isoxsuprine HCl (Isox), (p) dopamine HCl (Dopa) and (q) aminoguanidine HCl (Amin).

Figure 1. Correlations between experimental and calculated values of (a) C_Q and (b) η_Q . All calculations were completed using CASTEP after geometry optimization of the all of the atomic positions. The solid line is the line of best fit for the plotted points and the dashed line represents perfect correlation.

Figure 2. ^{35}Cl SSNMR spectra of (a) Adip, (b) Bufl, (c) Dicy and (d) Trig. Experimental spectra are shown in black, and corresponding analytical simulations are shown in red. Spinning sidebands are denoted by asterisks (*).

Figure 3. ^{35}Cl EFG tensor orientation of (a) Adip, (b) Bufl, (c) Dicy and (d) Trig. The short ($< 2.6 \text{ \AA}$) chlorine-hydrogen contacts are shown in red, and longer contacts are marked with dashed lines. Hydrogen atoms greater than 3.0 \AA from the chlorine anion have been deleted for clarity. In each case, two components of the EFG tensor are oriented in the plane of the paper, with the remaining component perpendicular to the page. This formalism is used for all pictures of the EFG tensors herein.

Figure 4. ^{35}Cl SSNMR spectra of (a) Rani, (b) Dibu, (c) Scop and (d) Mexi. Experimental spectra are shown in black, and corresponding analytical simulations are shown in red. Spinning sidebands are denoted by *.

Figure 5. ^{35}Cl EFG tensor orientation of (a) Scop and (b) Rani. V_{33} is oriented approximately perpendicular to the plane formed by the Cl atom and its two shortest H contacts (i.e., the $\text{H}\cdots\text{C}\cdots\text{H}$ plane).

Figure 6. ^{35}Cl SSNMR spectra of Brom. Experimental spectra shown in black, corresponding analytical simulations are shown in red. Spinning sidebands are denoted by *.

Figure 7. ^{35}Cl EFG tensor orientation of Brom. V_{33} is oriented near to the direction of the closest hydrogen contact ($\angle(V_{33}\text{-Cl-H}) = 16.14^\circ$).

Figure 8. ^{35}Cl SSNMR spectra of (a) Alpr, (b) Isop, (c) Aceb and (d) Aman. Experimental spectra are shown in black, and corresponding analytical simulations are shown in red. Spinning sidebands are denoted by *.

Figure 9. ^{35}Cl EFG tensor orientation of (a) Alpr, (b) Isop, (c) Aceb and (d) Aman. V_{11} and V_{22} are oriented near the directions of the two shortest contacts. Unlike the cases of the one- and two-contact systems, there does not seem to be a universally occurring tensor orientation (see

text for details on other systems).

Figure 10. ^{35}Cl SSNMR spectra of Proc. Experimental spectra shown in black, corresponding analytical simulations are shown in red. Spinning sidebands are denoted by *.

Figure 11. ^{35}Cl EFG tensor orientation of Proc. V_{33} (which is negative, as in the one contact systems) is directed toward the shortest $\text{NH}\cdots\text{Cl}$ contact ($(\angle(V_{33}\text{-Cl-H}) = 14.83^\circ)$).

Figure 12. ^{35}Cl SSNMR spectra of (a) Isox, (b) Dopa and (c) Amin. Experimental spectra are shown in black, and corresponding analytical simulations are shown in red. Spinning sidebands are denoted by *.

Figure 13. ^{35}Cl EFG tensor orientations of (a) Dopa and (b) Amin. For Dopa, V_{33} is directed toward the shortest $\text{H}\cdots\text{Cl}$ contact ($(\angle(V_{33}\text{-Cl-HO}) = 15.67^\circ)$). Dopa has a large magnitude of C_Q , and V_{33} is calculated as positive (i.e., negative C_Q), just like in the one-contact systems. For Amin, V_{33} is not directed near a short $\text{H}\cdots\text{Cl}$ contact, but rather, points into areas where there are no nearby hydrogen atoms. There are no short contacts less than 2.2 Å, there are no oxygen-containing moieties making hydrogen bonding contact, and accordingly, V_{33} is calculated as negative (i.e., positive C_Q).

Figure 14. ^{35}Cl SSNMR spectra of (a) Isox and (b) IsoxI. Experimental spectra shown in black, and corresponding analytical simulations are shown in red. Spinning sidebands are denoted by *.

Figure 15. ^{35}Cl EFG tensor orientations of (a) Isox, (b) IsoxI site 1, and (c) IsoxI site 2. See text for a detailed discussion.

Figure 16. ^{35}Cl SSNMR spectra of (a) Mexi and (b) MexiI. Experimental spectra are shown in black, and corresponding analytical simulations are shown in red.

Figure 17. ^{35}Cl static SSNMR spectrum of MexiII acquired at 9.4 T.

Figure 18. ^{35}Cl EFG tensor orientations of (a) Mexi site 1 and (b) Mexi site 2.

Table 1. Experimental and theoretical ^{35}Cl EFG and CS tensor parameters for HCl pharmaceuticals with one and two close H...Cl contacts.

		C_Q (MHz) ^a	η_Q ^b	δ_{iso} (ppm) ^c	Ω (ppm) ^d	κ ^e	α (°) ^f	β (°) ^f	γ (°) ^f
Adip	Exp.	5.94(6)	0.18(3)	128(5)	155(20)	0.60(20)	10(10)	13(2)	35(15)
	Calc.	-7.34	0.14	103	160	0.84	170	13	336
Bufl	Exp.	5.67(13)	0.18(6)	75(10)	125(30)	-0.60(20)	5(5)	8(4)	45(10)
	Calc.	-7.68	0.16	39	122	-0.15	177	13	137
Dicy	Exp.	5.80(5)	0.45(1)	52(4)	100(10)	0.00(20)	90(2)	10(1)	40(4)
	Calc.	-7.62	0.40	98	140	-0.15	301	18	127
Trig	Exp.	7.50(12)	0.05(3)	70(10)	120(30)	0.80(20)	30(20)	12(5)	50(15)
	Calc.	-9.61	0.16	84	194	0.42	345	8	314
Rani	Exp.	4.70(10)	0.92(3)	75(5)	70(15)	0.30(30)	55(10)	95(10)	10(10)
	Calc.	5.71	0.81	55	71	-0.17	90	94	90
Mexi site 1	Exp.	5.45(10)	0.40(8)	90(5)	80(20)	-0.80(20)	40(30)	100(20)	0(20)
	Calc.	7.23	0.29	77	109	-0.81	26	78	10
Dibu Site 1	Exp.	4.65(20)	0.86(7)	105(15)	100(20)	-0.26(60)	70(15)	80(50)	90(10)
	Calc. ^g	----	----	----	----	----	----	----	----
Scop	Exp.	3.82(3)	0.99(1)	0(4)	50(4)	-1.00(30)	90(9)	0(10)	0(6)
	Calc.	5.90	0.93	28	81	-0.30	215	65	159
Brom	Exp.	5.80(3)	0.04(1)	85(5)	90(10)	0.00(10)	0(20)	0(2)	0(23)
	Calc.	-7.63	0.26	116	126	0.14	136	11	296

The electric field gradient (EFG) tensor is described by three principal components such that $|V_{33}| \geq |V_{22}| \geq |V_{11}|$. ^a $C_Q = eQV_{33}/h$. The sign of C_Q cannot be determined from direct observation of the NMR spectrum of a quadrupolar nucleus, but is provided by theoretical methods; ^b $\eta_Q = (V_{11} - V_{22})/V_{33}$. The chemical shift (CS) tensor is described by three principal components such that $\delta_{11} \geq \delta_{22} \geq \delta_{33}$. $\delta_{jj} = \approx \sigma_{\text{iso,ref}} - \sigma_{jj}$, where $jj = 11, 22, 33$. $\sigma_{\text{iso,ref}}$ corresponds to the reference nuclear shielding, 971.22 ppm for ^{35}Cl , determined from calculations on NaCl. ^c $\delta_{\text{iso}} = (\delta_{11} + \delta_{22} + \delta_{33})/3$; ^d $\Omega = \delta_{11} - \delta_{33}$; ^e $\kappa = 3(\delta_{22} - \delta_{\text{iso}})/\Omega$. ^f The Euler angles, α , β and γ , define the relative orientation of the CS and EFG tensors. The “ZYZ” convention for rotation is used herein, as described by Dye et al.,⁵⁷ and as implemented in the WSolids⁷⁵ and EFGShield⁷⁹ software packages. Only EFG tensor parameters were calculated; CS tensor parameters were not obtained due to memory restrictions on the CASTEP calculations. ^g Unable to obtain EFG or CS tensor parameters due to the large unit cell size and limited computational resources.

Table 2. Experimental and theoretical ^{35}Cl EFG and CS tensor parameters for HCl pharmaceuticals with three and four or more close H \cdots Cl contacts.^a

		C_Q (MHz)	η_Q	δ_{iso} (ppm)	Ω (ppm)	κ	α ($^\circ$)	β ($^\circ$)	γ ($^\circ$)
Alpr	Exp.	5.25(2)	0.87(1)	60(1)	88(2)	0.00(20)	80(2)	97(2)	0(1)
	Calc.	6.42	0.96	75	142	0.09	92	79	214
Isop	Exp.	5.30(5)	0.93(4)	73(4)	90(3)	-1.00(10)	20(1)	5(1)	0(1)
	Calc.	7.63	0.88	82	128	0.45	289	84	348
Aceb	Exp.	4.57(5)	0.50(4)	95(5)	95(10)	-0.30(30)	15(5)	15(5)	60(5)
	Calc.	-5.51	0.81	129	61	0.32	315	83	113
Aman	Exp.	2.90(4)	0.68(3)	131(5)	50(5)	0.60(20)	80(10)	80(10)	20(20)
	Calc.	3.99	0.41	159	82	-0.35	39	79	4
Proc	Exp.	4.25(5)	0.52(2)	50(2)	60(10)	0.00(20)	72(6)	5(5)	1(1)
	Calc.	-5.17	0.85	90	127	-0.64	359	60	88
Isox	Exp.	5.50(15)	0.25(5)	120(10)	50(20)	0.50(40)	40(20)	55(15)	20(20)
	Calc.	6.75	0.17	104	52	0.32	130	50	187
Dopa	Exp.	5.10(14)	0.74(18)	33(7)	50(14)	0.00(50)	30(3)	0(5)	0(2)
	Calc.	-7.30	0.52	83	94	0.32	328	20	105
Mexi site 2	Exp.	3.10(10)	0.55(10)	130(5)	75(20)	0.80(20)	10(10)	5(5)	0
	Calc.	3.03	0.86	102	74	0.75	215	65	159
Amin	Exp.	2.0(2)	0.76(4)	50(3)	55(5)	0.45(15)	40(4)	70(2)	35(10)
	Calc.	3.37	0.38	92	84	-0.15	144	75	216

^a Definitions of EFG and CS tensor parameters are given in Table 1.

Table 3. Short H...Cl contacts and experimentally determined ^{35}Cl SSNMR parameters for HCl pharmaceuticals with one and two close H...Cl contacts.^a

Compound	Contact Type ^b	H...Cl Contacts (Å) ^c	C_Q (MHz)	η_Q	δ_{iso} (ppm)
Adip	R ₃ NH ⁺ ...Cl	2.037	5.94(6)	0.18(3)	128(5)
Bufl	R ₃ NH ⁺ ...Cl	1.957	5.67(13)	0.18(6)	75(10)
Dicy	R ₃ NH ⁺ ...Cl	1.956	5.80(5)	0.45(1)	52(4)
Trig	ROOH...Cl	1.883	7.50(12)	0.05(3)	70(10)
Tetr ⁵⁴	R ₃ NH ⁺ ...Cl	1.899	6.00(10)	0.27(4)	71(6)
Rani	R ₃ NH ⁺ ...Cl	2.023	4.70(10)	0.92(3)	75(5)
	R ₂ NH...Cl	2.185			
Dibu site 1 ^d	R ₃ NH ⁺ ...Cl	2.010	4.65(20)	0.86(7)	105(15)
	R ₂ NH...Cl	2.361			
Scop	ROH...Cl	2.101	3.82(3)	0.99(1)	0(4)
	R ₃ NH ⁺ ...Cl	2.111			
Mexi site 1	RNH ₃ ⁺ ...Cl	1.996	5.45(10)	0.40(8)	90(5)
	RNH ₃ ⁺ ...Cl	2.058			
Brom	R ₃ NH ⁺ ...Cl	2.020	5.80(3)	0.04(1)	85(5)
	RNH ₂ ...Cl	2.278			
Lido ⁵⁴	R ₃ NH ⁺ ...Cl	1.995	4.67(7)	0.77(3)	100(4)
	HOH...Cl	2.246			

^a Definitions of EFG and CS tensor parameters are given in Table 1. Values highlighted in grey are from previous work (reference numbers are next to compound names). ^b Indicates the functional group contributing to the H...Cl short contacts (i.e., RNH₃⁺ signifies a positively charged ammonium type hydrogen contact and ROH indicates an alcohol hydrogen contact). ^c The shortest H...Cl contacts (< 2.6 Å) as determined via energy minimization and geometry optimization with DFT plane wave calculations (see the experimental section for details). ^d Unable to perform a full or hydrogen-only geometry optimization due to the large unit cell size and limited computational resources.

Table 4. Short H...Cl contacts and experimentally determined ^{35}Cl SSNMR parameters for HCl pharmaceuticals with three close H...Cl contacts.^a

Compound	Contact Type ^b	H...Cl Contacts (Å) ^c	C_Q (MHz)	η_Q	δ_{iso} (ppm)
Alpr	R ₂ NH ₂ ⁺ ...Cl	2.036	5.25(2)	0.87(1)	60(1)
	R ₂ NH ₂ ⁺ ...Cl	2.159			
	ROH...Cl	2.250			
Isop	ROH...Cl	2.044	5.30(5)	0.930(4)	73(4)
	ROH...Cl	2.105			
	R ₂ NH ₂ ⁺ ...Cl	2.105			
Aceb	ROH...Cl	2.189	4.57(5)	0.50(4)	95(5)
	R ₂ NH ₂ ⁺ ...Cl	2.459			
Aman	R ₂ NH ₂ ⁺ ...Cl	2.168	2.90(4)	0.68(3)	131(5)
	RNH ₃ ⁺ ...Cl	2.124			
	RNH ₃ ⁺ ...Cl	2.135			
Proc	RNH ₃ ⁺ ...Cl	2.191	4.25(5)	0.52(2)	50(2)
	R ₃ NH ⁺ ...Cl	2.008			
	R ₂ NH...Cl	2.294			
Lcme ⁵⁷	RNH ₂ ...Cl	2.356	2.37(1)	0.81(3)	48.2(7)
	RNH ₃ ⁺ ...Cl	2.101			
	RNH ₃ ⁺ ...Cl	2.110			
	RNH ₃ ⁺ ...Cl	2.239			

^a Definitions of EFG and CS tensor parameters are given in Table 1. Values highlighted in grey are from previous work (reference numbers are next to compound names). ^b Indicates the functional group contributing to the H...Cl short contacts (i.e., RNH₃⁺ signifies a positively charged ammonium type hydrogen contact and ROH indicates an alcohol hydrogen contact). ^c The short H...Cl contacts (< 2.6 Å) as determined via energy minimization and geometry optimization with DFT plane wave calculations (see the experimental section for details).

Table 5. Short H...Cl contacts and experimentally determined ^{35}Cl SSNMR parameters for HCl pharmaceuticals with four or more close H...Cl contacts.^a

Compound	Contact Type ^b	H...Cl Contacts (Å) ^c	C_Q (MHz)	η_Q	δ_{iso} (ppm)
Isox	R ₂ NH ₂ ⁺ ...Cl	2.137	5.50(15)	0.25(5)	120(10)
	ROH...Cl	2.139			
	ROH...Cl	2.168			
Mexi site 2	R ₂ NH ₂ ⁺ ...Cl	2.383	3.10(10)	0.55(10)	130(5)
	RNH ₃ ⁺ ...Cl	2.123			
	RNH ₃ ⁺ ...Cl	2.138			
	RNH ₃ ⁺ ...Cl	2.318			
Dopa	RNH ₃ ⁺ ...Cl	2.342	5.10(14)	0.74(18)	33(7)
	ROH...Cl	2.096			
	RNH ₃ ⁺ ...Cl	2.174			
	ROH...Cl	2.178			
	RNH ₃ ⁺ ...Cl	2.234			
Amin	RNH ₃ ⁺ ...Cl	2.264	2.0(2)	0.76(4)	50(3)
	RNNH...Cl	2.208			
	RNH ₂ ...Cl	2.297			
	NNH ₂ ...Cl	2.347			
	NNH ₂ ...Cl	2.381			
	RNH ₂ ⁺ ...Cl	2.389			
Treo ⁹³	RNH ₂ ...Cl	2.562	5.4(1)	0.94(2)	99(10)
	ROH...Cl	1.998			
	RNH ₃ ⁺ ...Cl	2.189			
	ROH...Cl	2.202			
	RNH ₃ ⁺ ...Cl	2.227			

^a Definitions of EFG and CS tensor parameters are given in Table 1. Values highlighted in grey are from previous work (reference numbers are next to compound names). ^b Indicates the functional group contributing to the H...Cl short contacts (i.e., RNH₃⁺ signifies a positively charged ammonium type hydrogen contact and ROH indicates an alcohol hydrogen contact). ^c The shortest H...Cl contacts (< 2.6 Å) as determined via energy minimization and geometry optimization with DFT plane wave calculations (see the experimental section for details).

Table 6. Experimental and theoretical ^{35}Cl EFG and CS tensor parameters for HCl pharmaceutical polymorphs. ^a

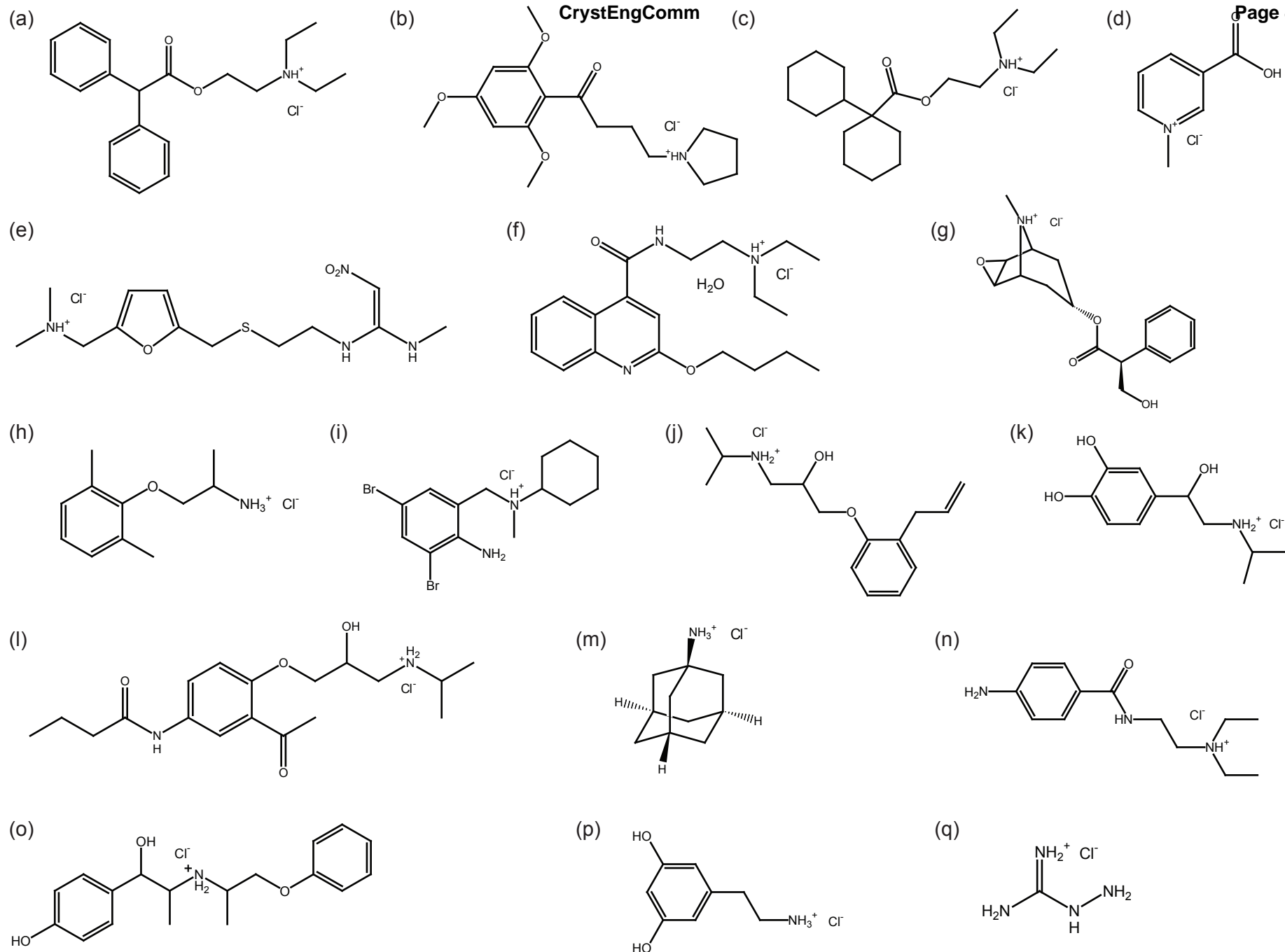
		C_Q (MHz)	η_Q	δ_{iso} (ppm)	Ω (ppm)	κ	α ($^\circ$)	β ($^\circ$)	γ ($^\circ$)
Isox	Exp.	5.50(15)	0.25(5)	120(10)	50(20)	0.50(40)	40(20)	55(15)	20(20)
	Calc.	6.75	0.17	104	52	0.32	50	50	173
IsoxI site 1	Exp.	6.5(1)	0.36(2)	80(3)	120(6)	-0.50(20)	50(4)	90(3)	150(5)
	Calc.	8.60	0.34	112	46	0.62	285	65	166
IsoxI site 2	Exp.	5.6(1)	0.33(1)	80(4)	175(20)	0.00(15)	60(5)	30(2)	90(4)
	Calc.	7.02	0.31	102	46	0.51	282	52	205
Mexi site 1	Exp.	5.45(10)	0.40(8)	90(5)	80(20)	-0.80(20)	40(30)	100(20)	0
	Calc.	7.23	0.29	77	109	-0.81	26	78	10
Mexi site 2	Exp.	3.10(10)	0.55(10)	130(5)	75(20)	0.80(20)	10(10)	5(5)	0
	Calc.	3.03	0.86	102	74	0.75	264	88	131
MexiI ^b	Exp.	1.99(10)	0.62(3)	55(4)	30(3)	-0.30(10)	92(5)	45(3)	50(10)
	Calc.	----	----	----	----	----	----	----	----
MexiII ^{b, c}	Exp.	----	----	----	----	----	----	----	----
	Calc.	----	----	----	----	----	----	----	----

^a Definitions of EFG and CS tensor parameters are given in Table 1. ^b No crystal structure available. ^c Accurate determination of the ^{35}Cl NMR parameters via analytical simulation is not possible due to the broad and featureless ^{35}Cl powder pattern.

Table 7. Short H...Cl contacts and experimentally determined ^{35}Cl SSNMR parameters for HCl pharmaceutical polymorphs.^a

Compound	Contact Type ^b	H...Cl Contacts (Å) ^c	C_Q (MHz)	η_Q	δ_{iso} (ppm)
Isox	ROH...Cl	2.137	5.50(15)	0.25(5)	120(10)
	R ₂ NH ₂ ⁺ ...Cl	2.139			
	ROH...Cl	2.168			
	R ₂ NH ₂ ⁺ ...Cl	2.383			
IsoxI site 1	R ₂ NH ₂ ⁺ ...Cl	2.087	6.5(1)	0.36(2)	80(3)
	ROH...Cl	2.153			
	ROH...Cl	2.182			
	R ₂ NH ₂ ⁺ ...Cl	2.255			
IsoxI site 2	R ₂ NH ₂ ⁺ ...Cl	2.117	5.6(1)	0.33(1)	80(4)
	ROH...Cl	2.121			
	ROH...Cl	2.191			
	R ₂ NH ₂ ⁺ ...Cl	2.420			
Mexi site 1	RNH ₃ ⁺ ...Cl	1.996	5.45(10)	0.40(8)	90(5)
	RNH ₃ ⁺ ...Cl	2.058			
Mexi site 2	RNH ₃ ⁺ ...Cl	2.123	3.10(10)	0.55(10)	130(5)
	RNH ₃ ⁺ ...Cl	2.138			
	RNH ₃ ⁺ ...Cl	2.318			
	RNH ₃ ⁺ ...Cl	2.342			
MexiI ^d	----	----	1.99(10)	0.62(3)	55(4)
MexiII ^{d, e}	----	----	----	----	----

^a Definitions of EFG and CS tensor parameters are given in Table 1. ^b Indicates the functional group contributing to the H...Cl short contacts (i.e., RNH₃⁺ signifies a positively charged ammonium type hydrogen contact and ROH indicates an alcohol hydrogen contact). ^c The shortest H...Cl contacts (< 2.6 Å) as determined via energy minimization and geometry optimization with DFT plane wave calculations (see the experimental section for details). ^d No crystal structure is available. ^e Accurate determination of the ^{35}Cl NMR parameters via analytical simulation is not possible due to the broad and featureless ^{35}Cl powder pattern.



Scheme 1. Schematic representations of (a) adiphenine HCl (Adip), (b) buflomedil HCl (Bufl), (c) dicyclomine HCl (Dicy), (d) trigonelline HCl (Trig), (e) ranitidine HCl (Rani), (f) dibucaine HCl (Dibu), (g) scopolamine HCl (Scop), (h) mexiletine HCl (Mexi), (i) bromhexine HCl (Brom), (j) alprenolol HCl (Alpr), (k) isoprenaline HCl (Isop), (l) acebutolol HCl (Aceb), (m) amantadine HCl (Aman), (n) procainamide HCl (Proc), (o) isoxsuprine HCl (Isox), (p) dopamine HCl (Dopa) and (q) aminoguanidine HCl (Amin).

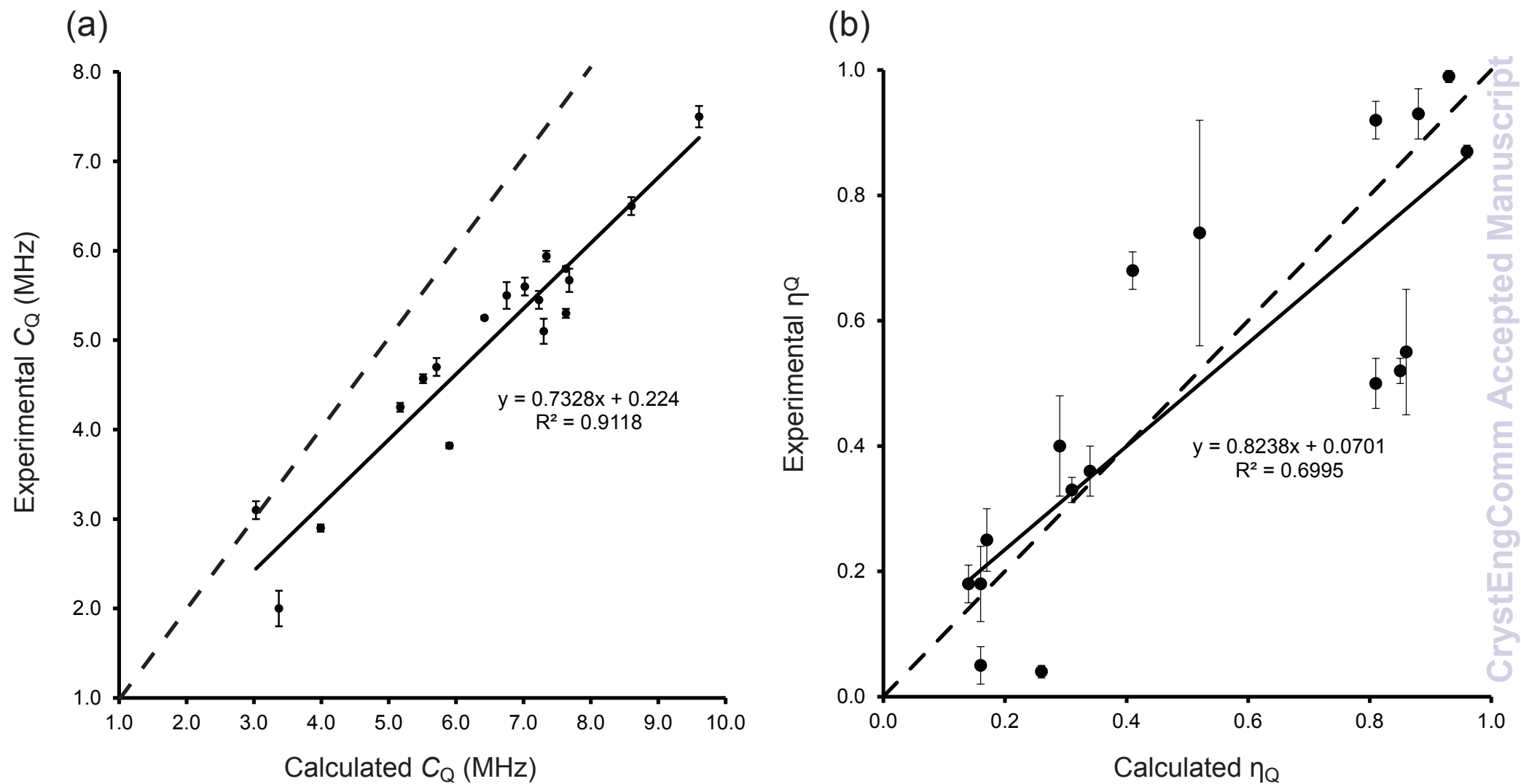


Figure 1. Correlations between experimental and calculated values of (a) C_Q and (b) η_Q . All calculations were completed using CASTEP after geometry optimization of the all of the atomic positions. The solid line is the line of best fit for the plotted points and the dashed line represents perfect correlation.

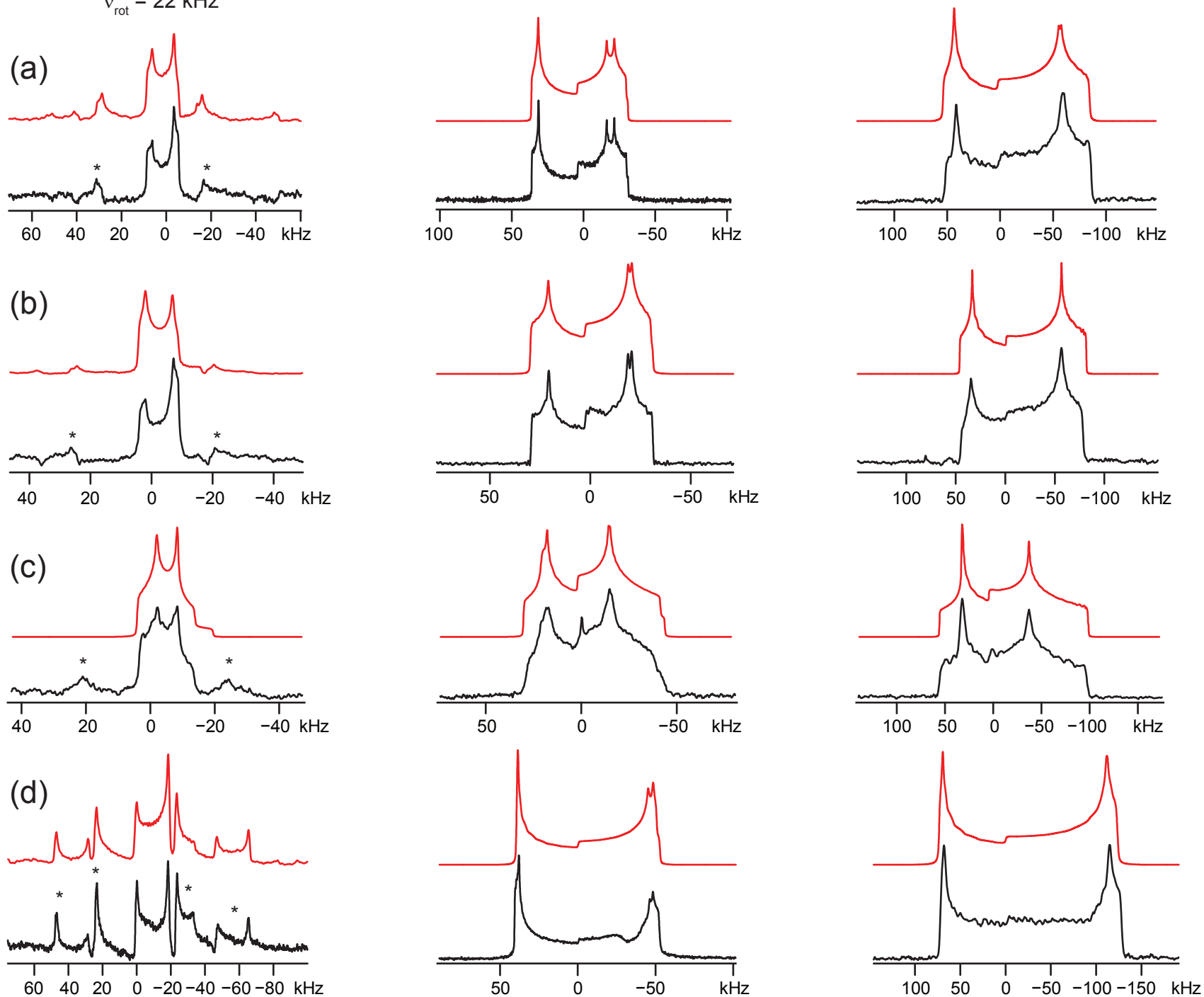


Figure 2. ^{35}Cl SSNMR spectra of (a) Adip, (b) Bufl, (c) Dicy and (d) Trig. Experimental spectra are shown in black, and corresponding analytical simulations are shown in red. Spinning sidebands are denoted by asterisks (*).

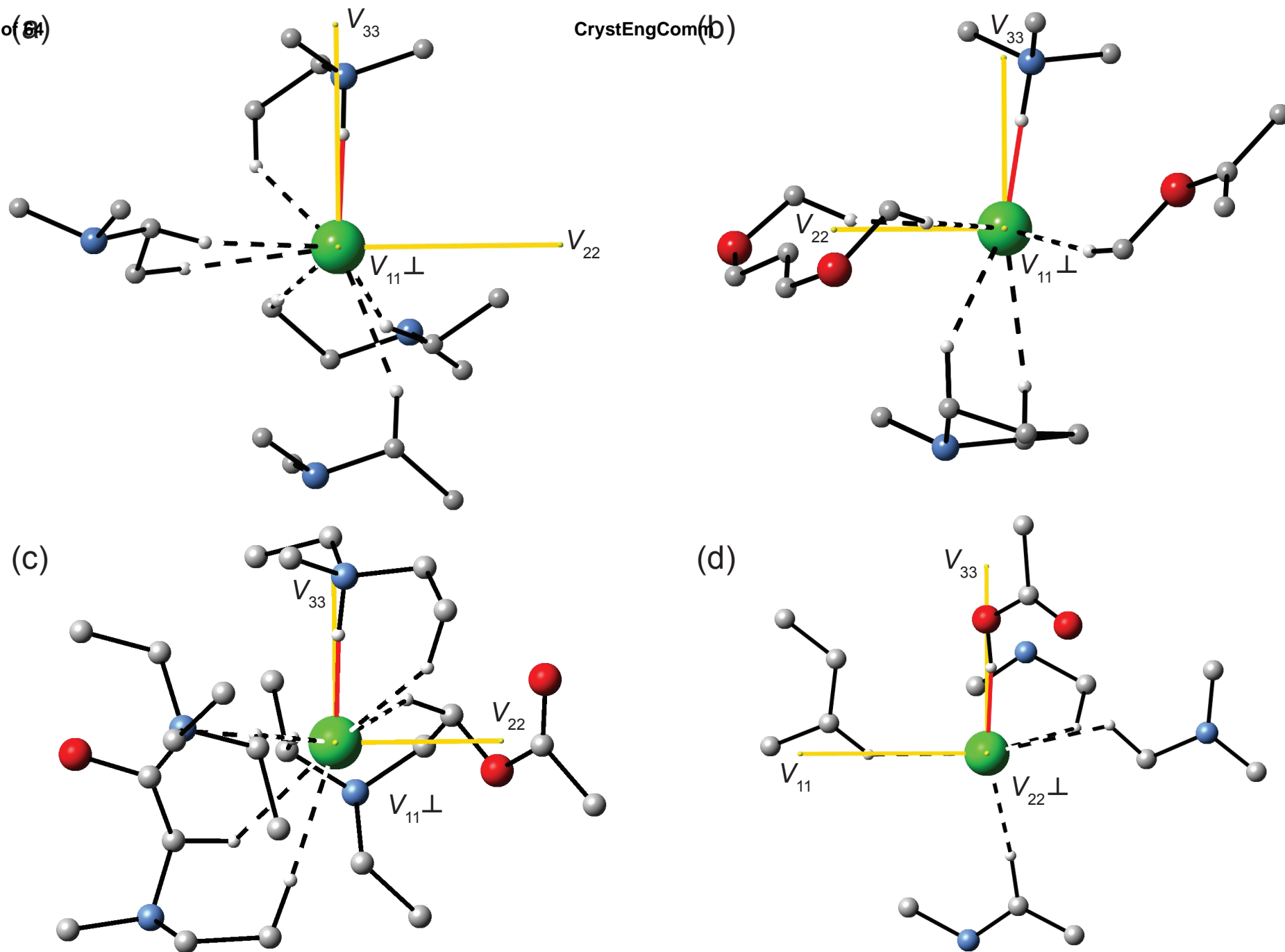


Figure 3. ^{35}Cl EFG tensor orientation of (a) Adip, (b) Bufl, (c) Dicy and (d) Trig. The short ($< 2.6 \text{ \AA}$) chlorine-hydrogen contacts are shown in red, and longer contacts are marked with dashed lines. Hydrogen atoms greater than 3.0 \AA from the chlorine anion have been deleted for clarity. In each case, two components of the EFG tensor are oriented in the plane of the paper, with the remaining component perpendicular to the page. This formalism is used for all pictures of the EFG tensors herein.

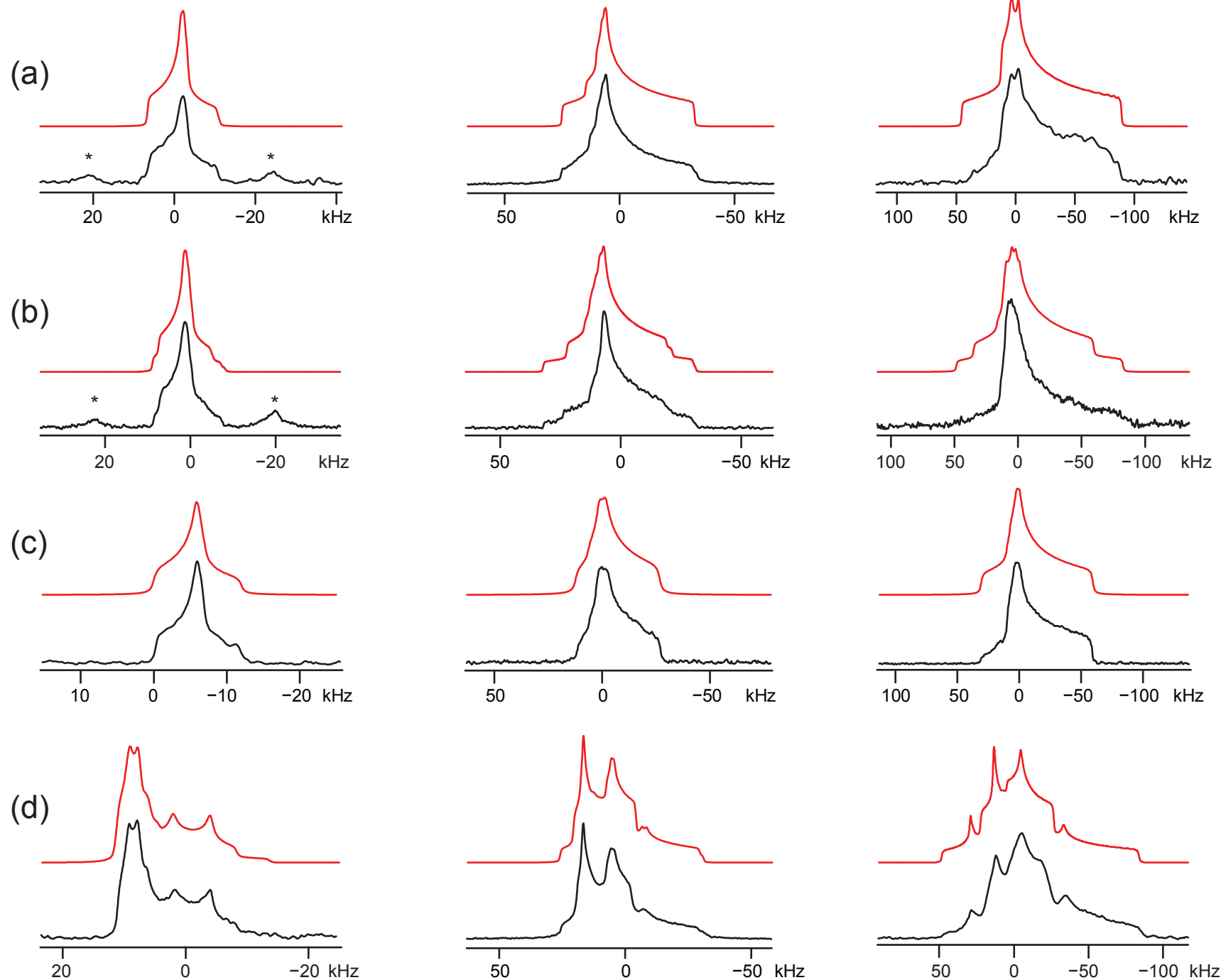


Figure 4. ^{35}Cl SSNMR spectra of (a) Rani, (b) Dibu, (c) Scop and (d) Mexi. Experimental spectra are shown in black, and corresponding analytical simulations are shown in red. Spinning sidebands are denoted by *.

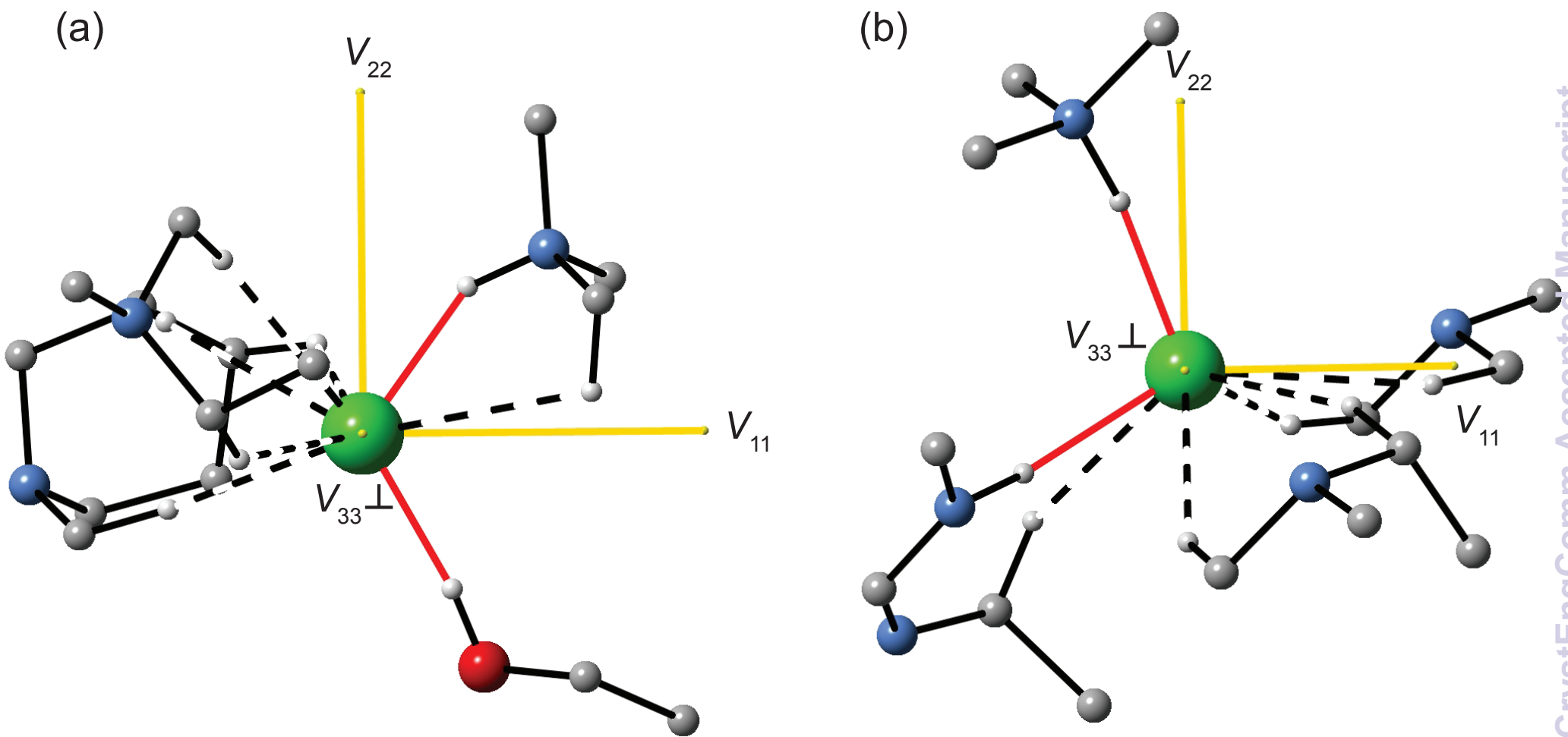


Figure 5. ^{35}Cl EFG tensor orientation of (a) Scop and (b) Rani. V_{33} is oriented approximately perpendicular to the plane formed by the Cl atom and its two shortest H contacts (i.e., the $\text{H}\cdots\text{C}\cdots\text{H}$ plane).

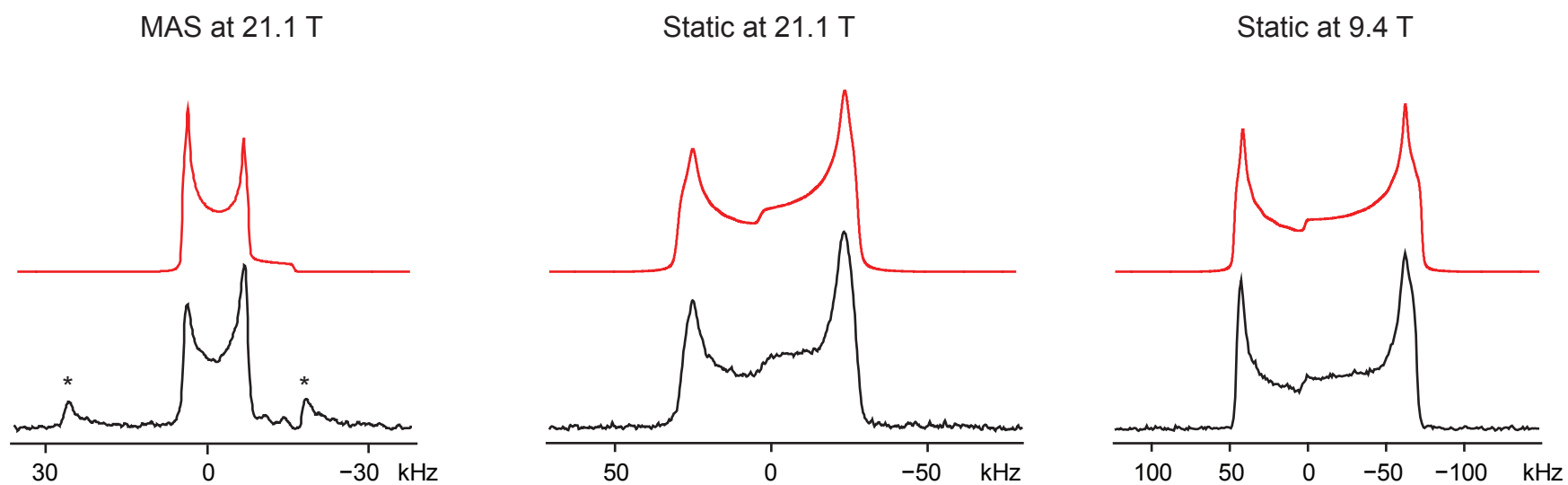


Figure 6. ^{35}Cl SSNMR spectra of Brom. Experimental spectra shown in black, corresponding analytical simulations are shown in red. Spinning sidebands are denoted by *.

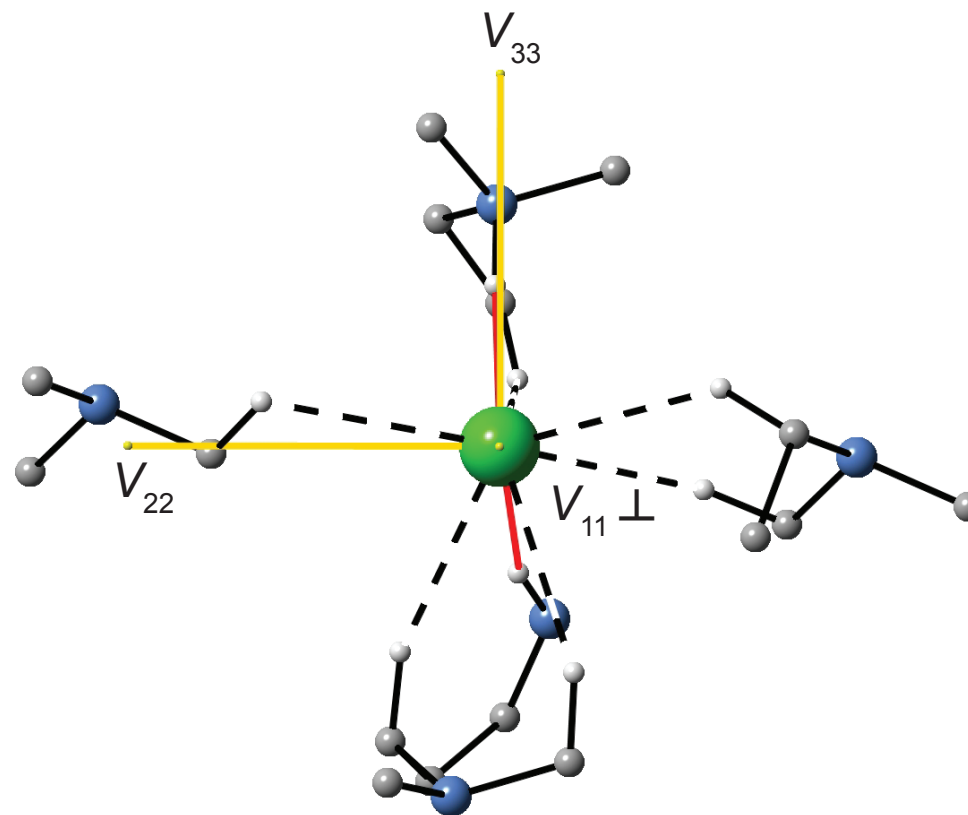


Figure 7. ^{35}Cl EFG tensor orientation of Brom. V_{33} is oriented near to the direction of the closest hydrogen contact ($\angle(V_{33}\text{-Cl-H}) = 16.14^\circ$).

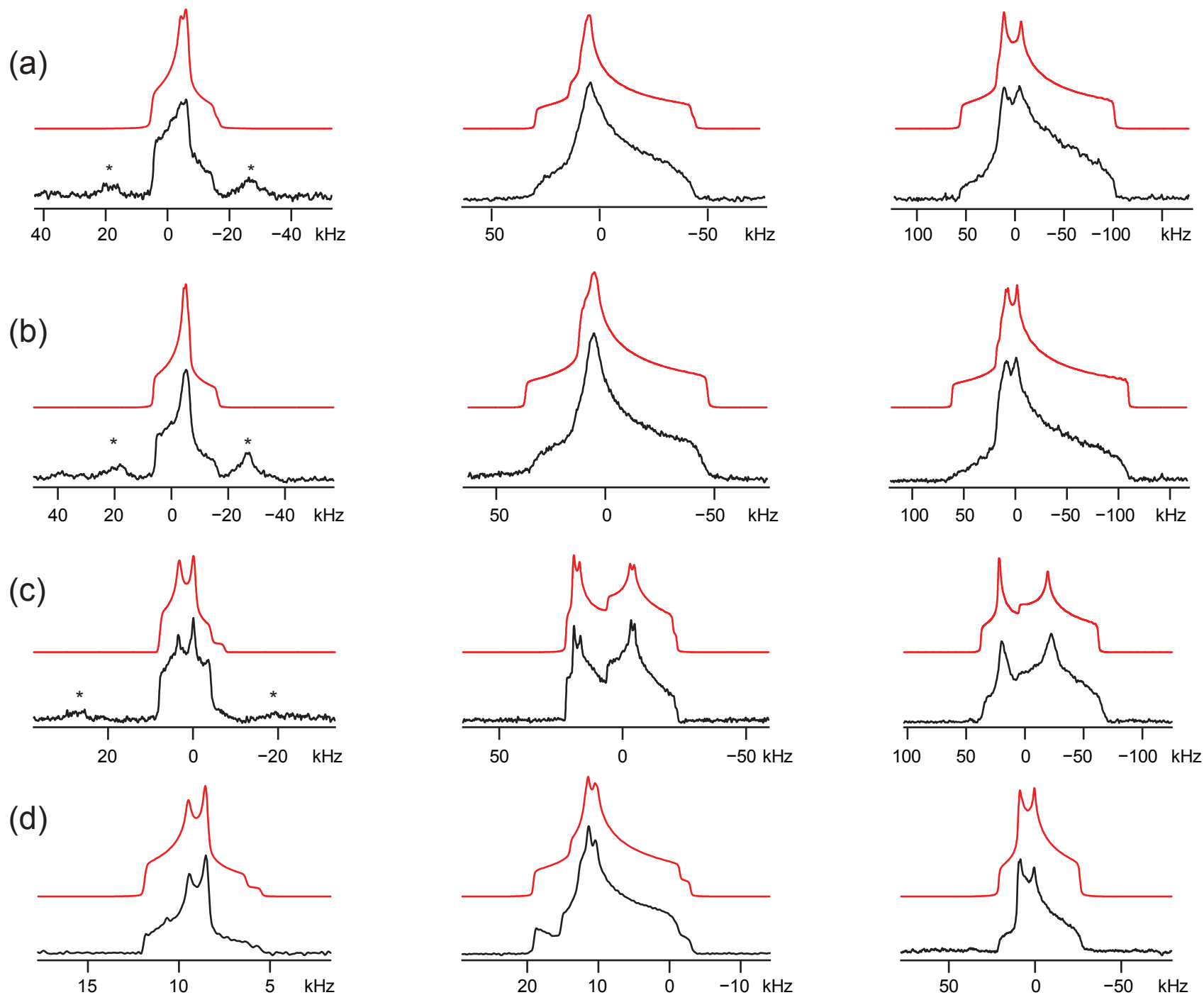
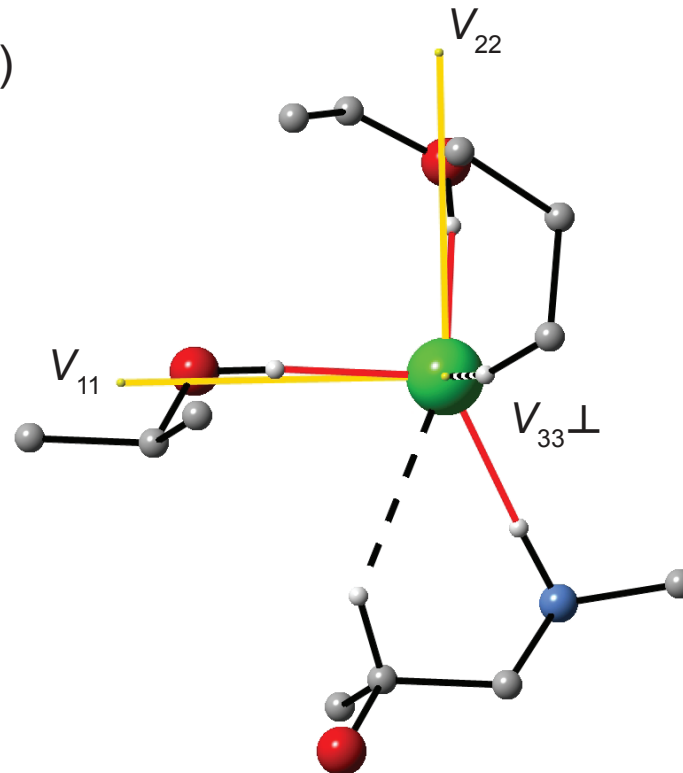
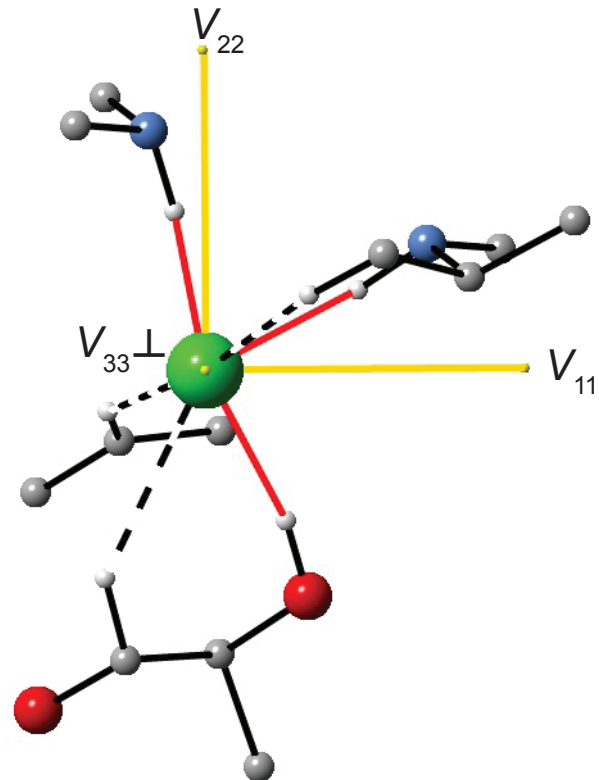
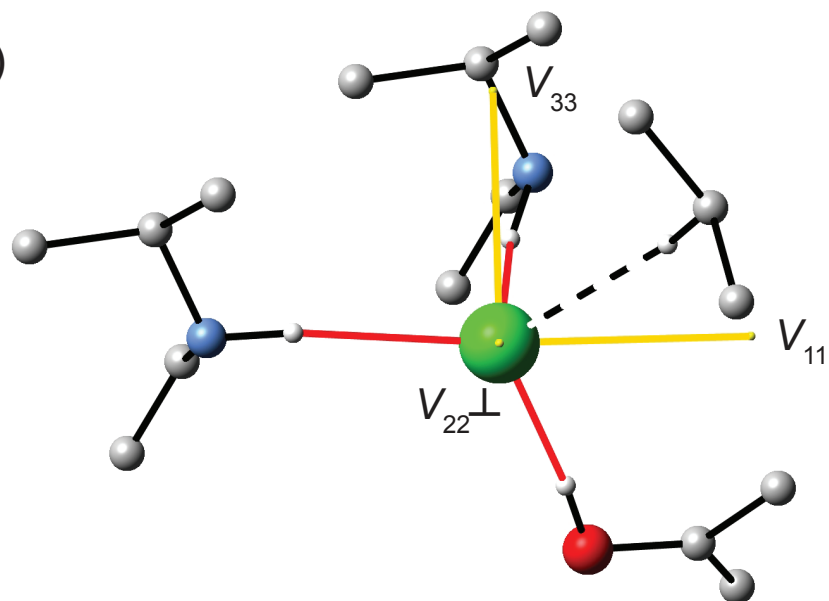


Figure 8. ^{35}Cl SSNMR spectra of (a) Alpr, (b) Isop, (c) Aceb and (d) Aman. Experimental spectra are shown in black, and corresponding analytical simulations are shown in red. Spinning sidebands are denoted by *.



(c)



(d)

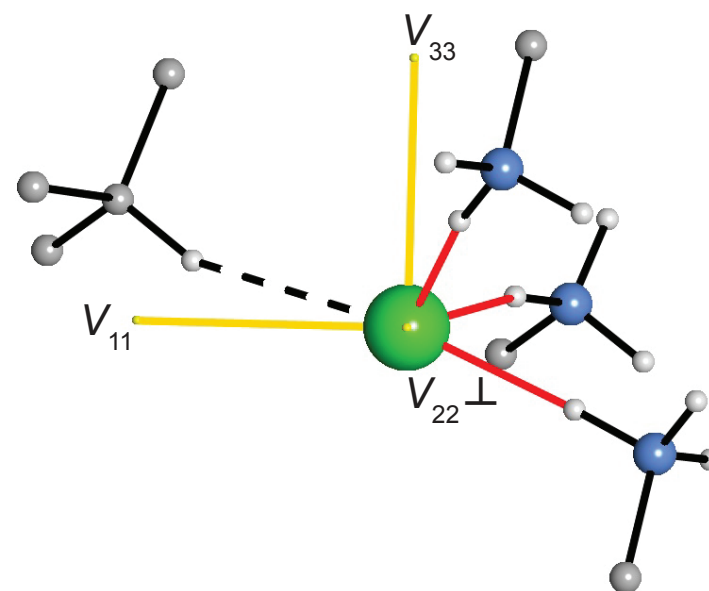


Figure 9. ^{35}Cl EFG tensor orientation of (a) Alpr, (b) Isop, (c) Aceb and (d) Aman. V_{11} and V_{22} are oriented near the directions of the two shortest contacts. Unlike the cases of the one- and two-contact systems, there does not seem to be a universally occurring tensor orientation (see text for details on other systems).

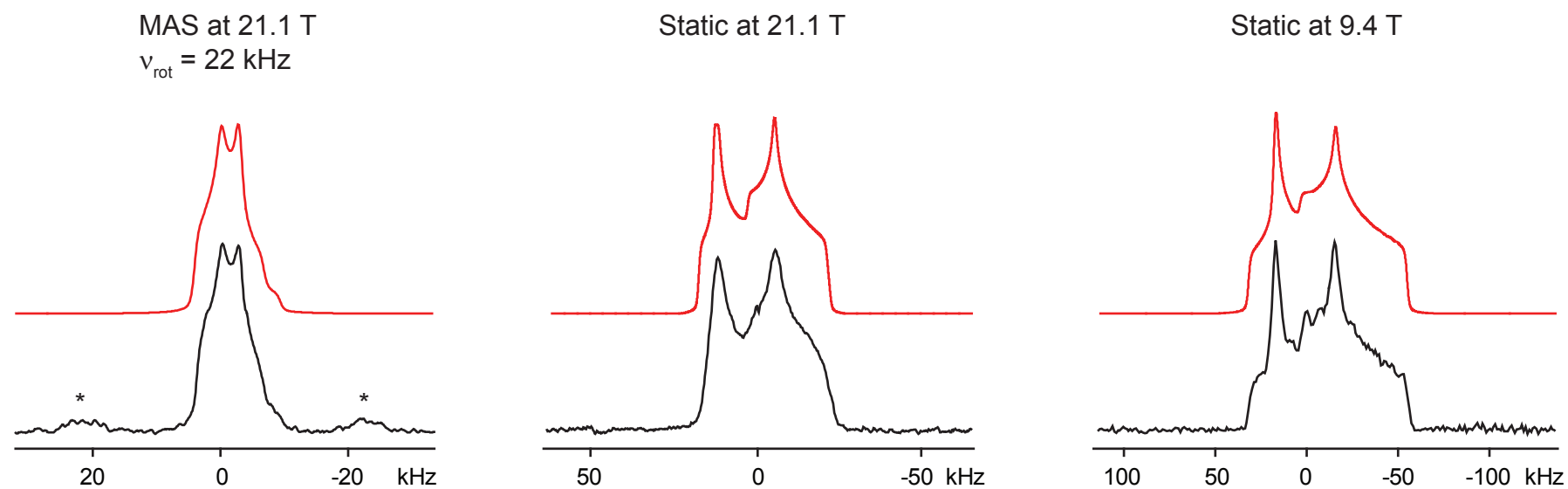


Figure 10. ^{35}Cl SSNMR spectra of Proc. Experimental spectra shown in black, corresponding analytical simulations are shown in red. Spinning sidebands are denoted by *.

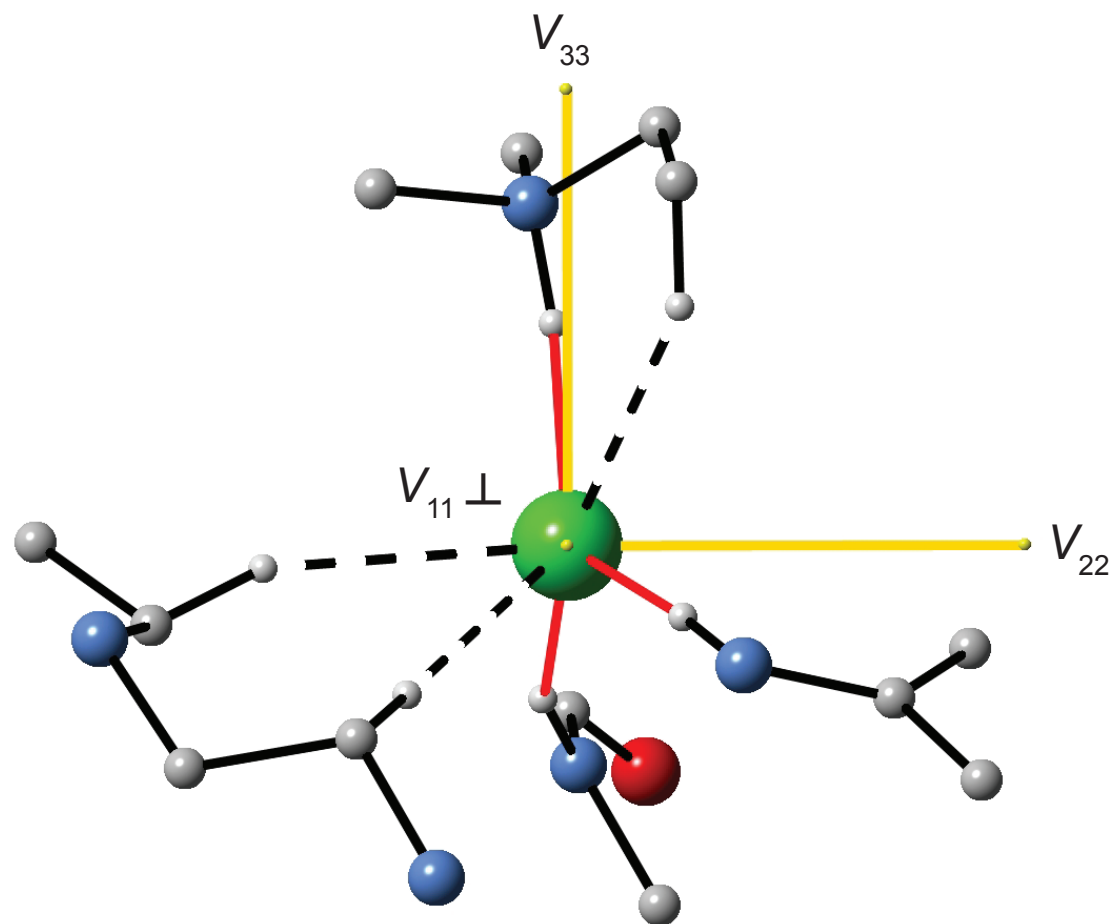


Figure 11. ^{35}Cl EFG tensor orientation of Proc. V_{33} (which is negative, as in the one contact systems) is directed toward the shortest $\text{NH}\cdots\text{Cl}$ contact ($\angle(V_{33}\text{-Cl-H}) = 14.83^\circ$).

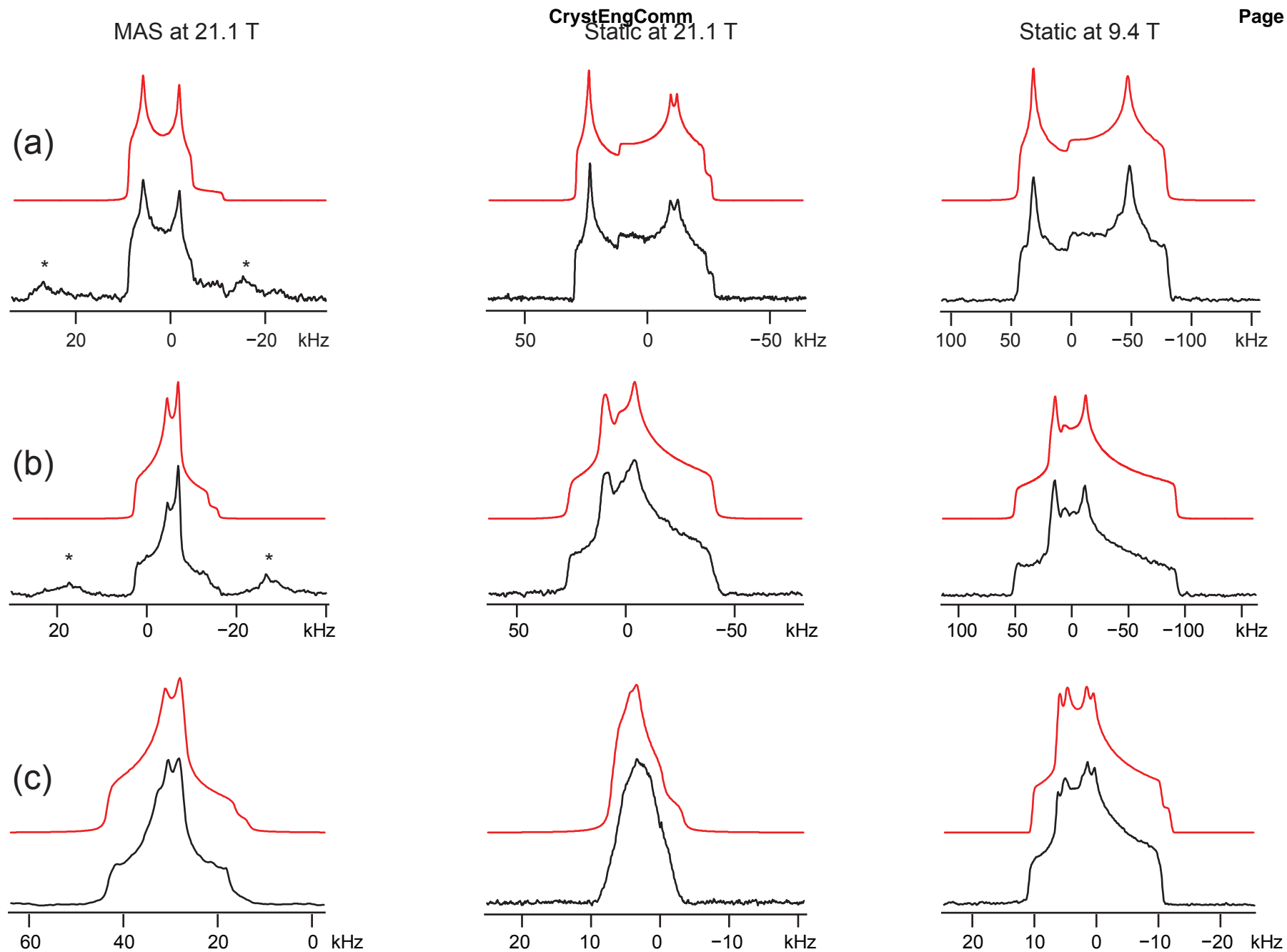


Figure 12. ^{35}Cl SSNMR spectra of (a) Isox, (b) Dopa and (c) Amin. Experimental spectra are shown in black, and corresponding analytical simulations are shown in red. Spinning sidebands are denoted by *.

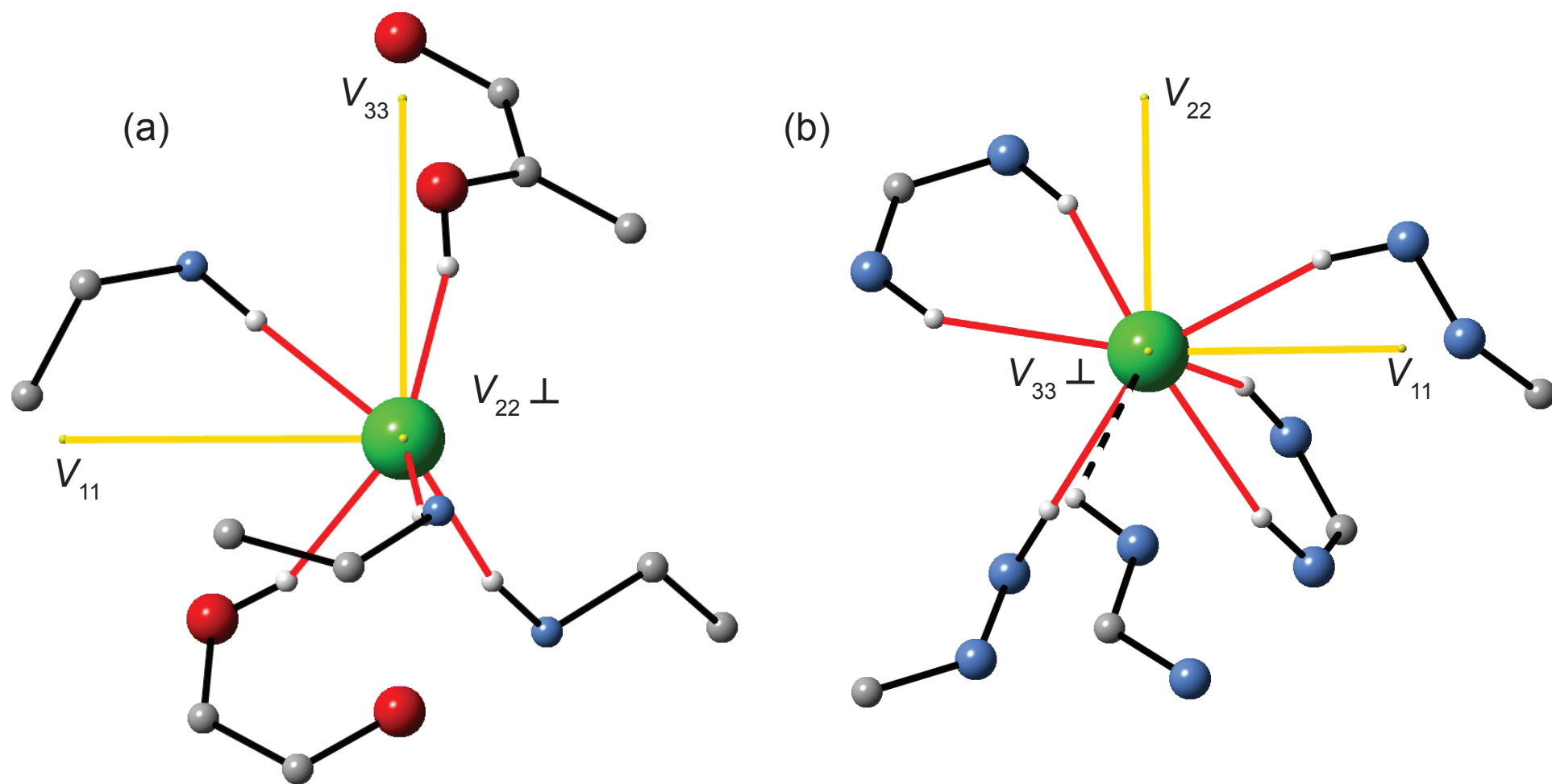


Figure 13. ^{35}Cl EFG tensor orientations of (a) Dopa and (b) Amin. For Dopa, V_{33} is directed toward the shortest $\text{H}\cdots\text{Cl}$ contact ($\angle(V_{33}\text{-Cl-HO}) = 15.67^\circ$). Dopa has a large magnitude of C_Q , and V_{33} is calculated as positive (i.e., negative C_Q), just like in the one-contact systems. For Amin, V_{33} is not directed near a short $\text{H}\cdots\text{Cl}$ contact, but rather, points into areas where there are no nearby hydrogen atoms. There are no short contacts less than 2.2 \AA , there are no oxygen-containing moieties making hydrogen bonding contact, and accordingly, V_{33} is calculated as negative (i.e., positive C_Q).

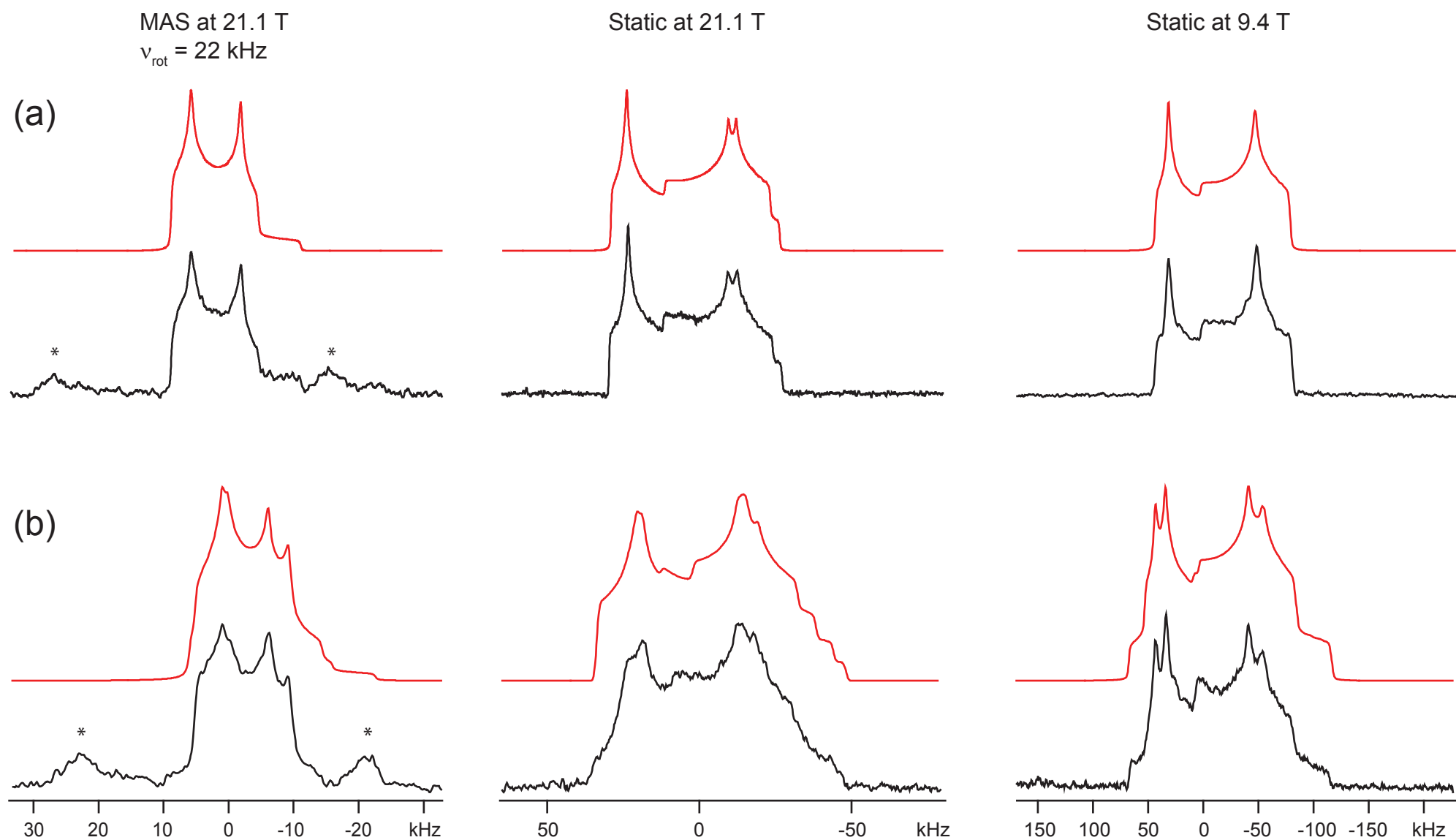


Figure 14. ^{35}Cl SSNMR spectra of (a) Isox and (b) IsoxI. Experimental spectra shown in black, and corresponding analytical simulations are shown in red. Spinning sidebands are denoted by *.

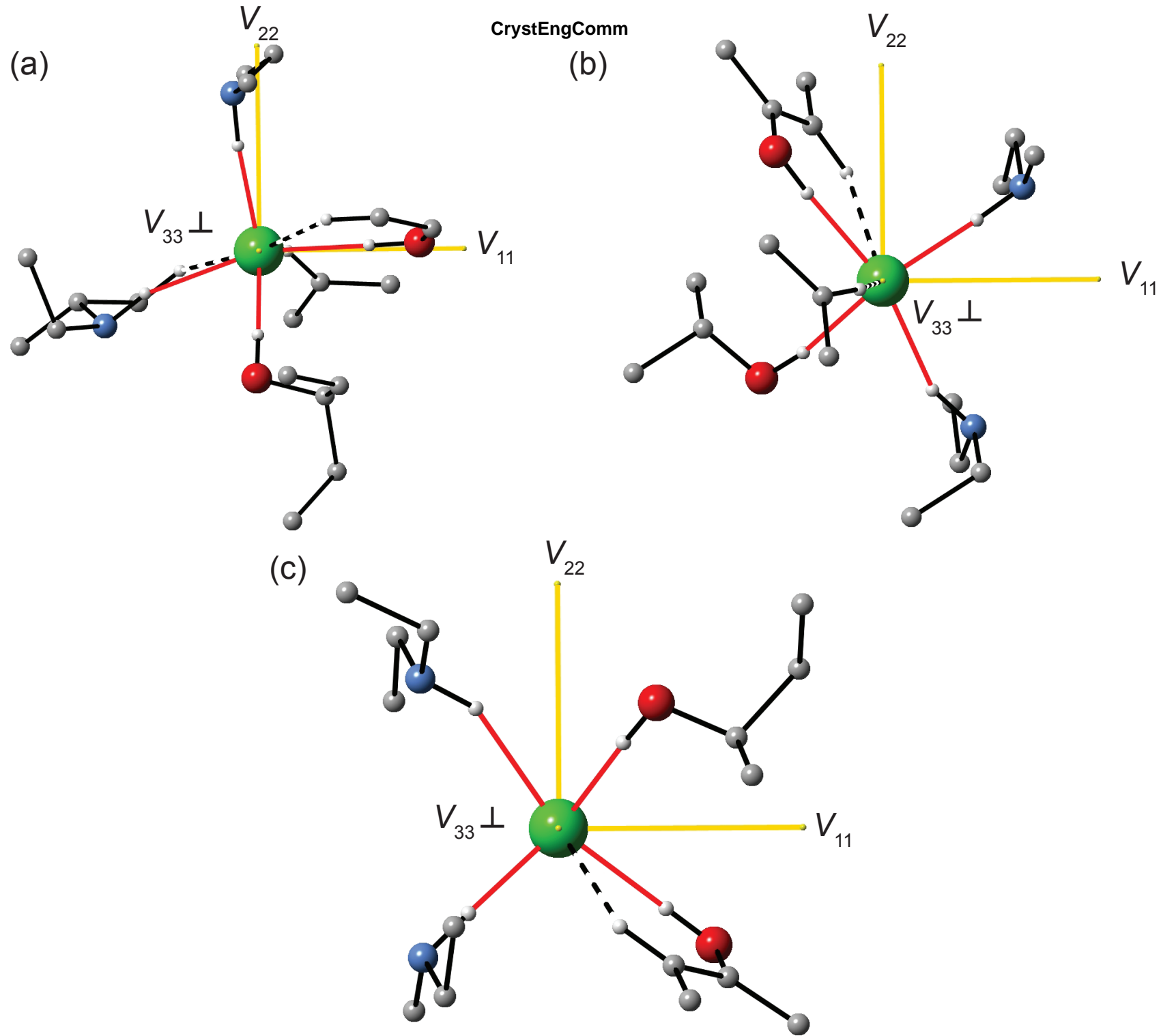


Figure 15. ^{35}Cl EFG tensor orientations of (a) Isox, (b) IsoxI site 1, and (c) IsoxI site 2. See text for a detailed discussion.

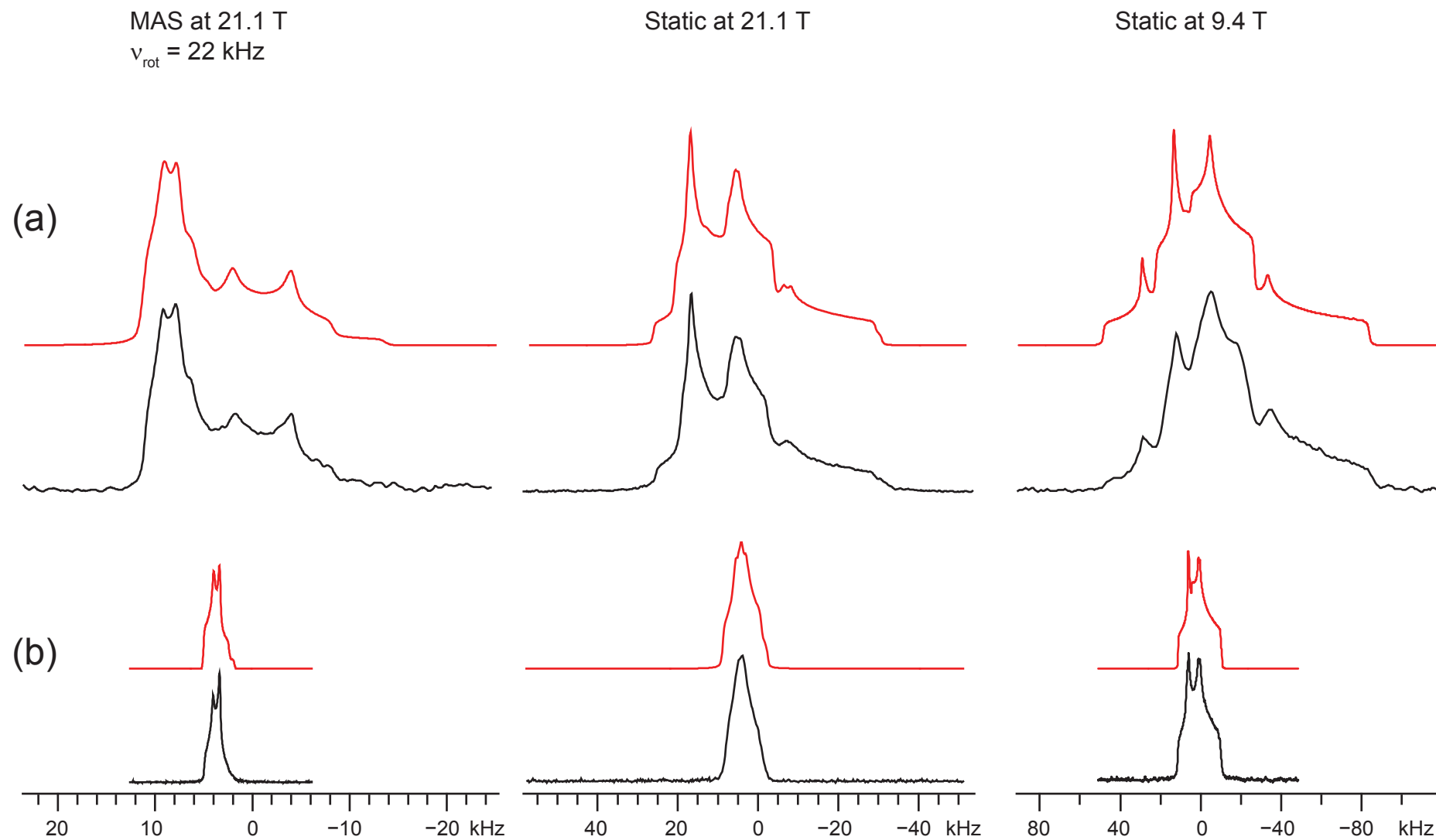


Figure 16. ^{35}Cl SSNMR spectra of (a) Mexi and (b) MexiI. Experimental spectra are shown in black, and corresponding analytical simulations are shown in red.

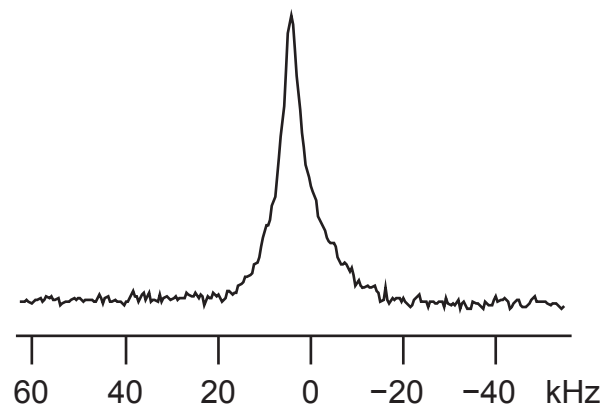


Figure 17. ^{35}Cl static SSNMR spectrum of MexiII acquired at 9.4 T.

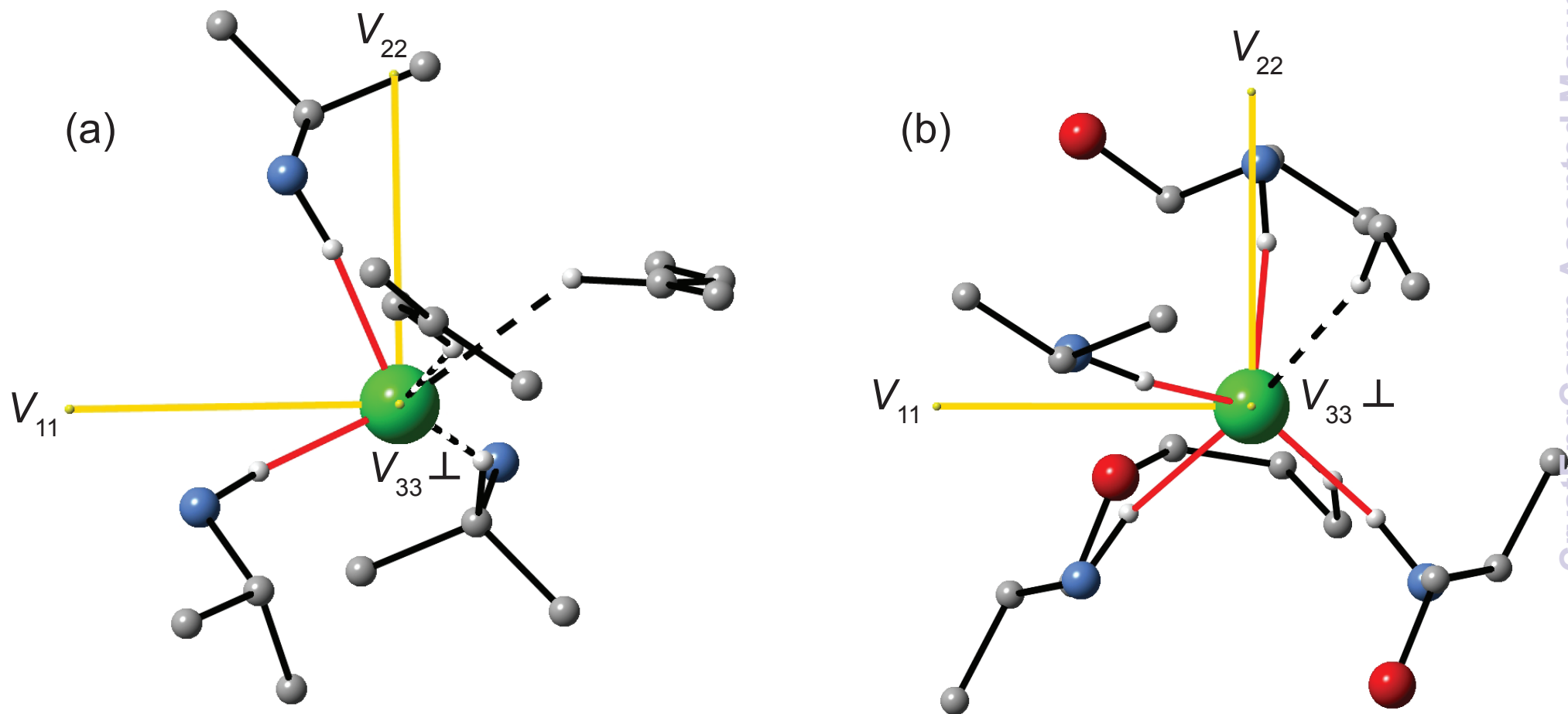


Figure 18. ^{35}Cl EFG tensor orientations of (a) Mexi site 1 and (b) Mexi site 2.